Politecnico di Milano

SCUOLA DI INGEGNERIA INDUSTRIALE E DELL'INFORMAZIONE
Corso di Laurea Magistrale in Ingegneria Fisica

Tesi di laurea magistrale

Meso-Superstructured Solar Cell based on Organo-Metal Halide Perovskite

Candidato:
Andrea Del Quarto
Matr. 798005

Relatore:
Prof. Guglielmo Lanzani

Correlatore:
Ing. Annamaria Petrozza

Anno Accademico 2014–2015

Contents

List of Figures

List of Tables

Abstract

In the last ten years, the photovoltaic field has been interested by an intense research activity, in order to develop new technologies which can guarantee good performance with more accessible cost. Today, the most part of the efforts are focused on developing devices realised through the "*solution processing*", which deletes the huge process costs characterizing the traditional technologies.
With this perspective, the *semi-organic* solar cell has demonstrated huge potential, joining the good optoelectronic properties of metals to the simplicity of the process related to organic materials.
Now the *Dye Sentitized Solar Cells* (DSSC) and *Meso-Superstructured Solar Cells* (MSSC), represent two of the most promising technologies, thanks to their high performance, already obtained since the first tests. The first devices that have given good results have been the liquid DSSC (Gratzel cell), in which a nanostructured semiconductor, usually TiO_2, is covered by optically active material (dye) and immersed in a liquid electrolyte. Thanks to the improvement of the architecture and the process, the MSSC technology has been developed; in particular the semiconductor has been replaced with nanostructured insulator. These cells using *Organo-Metal Halide Perovskite* as absorbing material, have reached a higher efficiency of 16%.
Although the photophysic dynamics are not known yet, recent studies have showed that the merit of these performance is attributable to the exceptional optoelectronic properties of the *Perovskite*. Indeed the potentiality of this material are not totally exploited by currently architecture, which, on the contrary, limits it.
At the beginning, the aim of this project was the realization of MSSC devices, through which to compare the performance of different architectures. In particular, the classic Hole Transport Layer (HTL) (Spiro-oMETAD) has been replaced with the *Molybdenum disulphide* (MoS_2), having better properties and low costs.
For the realization of the HTL of MoS_2, have been tested two different architectures:

- Uniform film formed by interconnected flakes of MoS_2
- Flakes of MoS_2 dispersed in an insulating matrix (PVP)

Nowadays, always with the target to take full advantage by the Perovskite's properties, several studies point to eliminate the HTL, in order to reduce the leakages of photocurrent due to absorber/HTL interface.

Sommario

Negli ultimi dieci anni, il settore fotovoltaico è stato interessato da una intensa attività di ricerca, atta allo sviluppo di nuove tecnologie che potessero garantire buone prestazioni ad un costo più accessibile. Attualmente gran parte degli sforzi sono concentrati sullo sviluppo di dispositivi realizzabili attraverso il così detto "*solution processing*", il quale evita gli enormi costi di processo che caratterizzano le tecnologie odierne.
In quest'ottica, le celle *semi-organiche* hanno dimostrato enormi potenzialità, unendo le proprietà optoelettroniche dei metalli alla semplicità di processo legata ai materiali organici.
Attualmente le *Dye Sentitized Solar Cells* (DSSC) e *Meso-Superstructured Solar Cells* (MSSC), rappresentano due tra le tecnologie più promettenti, grazie anche alle loro alte prestazioni, ottenute già dalle prime sperimentazioni. I primi dispositivi a fornire buoni risultati sono state le DSSC a stato liquido (celle di Gratzel), in cui un semiconduttore nanostrutturato, tipicamente TiO_2, era ricoperto da un materiale otticamente attivo (dye) ed immerso in un elettrolita liquido. Attraverso l'ingegnerizzazione dell'architettura e il miglioramento del processo, si è successivamente sviluppata la tecnologia MSSC, in cui si è sostituito il semiconduttore con un isolante nanostrutturato. Seppur con limitata riproducibilità, queste celle, impieganti come materiale attivo uno strato di *Organo-Metal Halide Perovskite*, hanno raggiunto efficienze superiori al 16%.
Sebbene le dinamiche della fotofisica non siano ancora chiare, da recenti studi è emerso che il merito di queste prestazioni è attribuibile in larga misura alle eccezionali proprietà optoelettroniche della *Perovskite*. Si pensa, infatti, che le potenzialità di questo materiale non siano sfruttate appieno dall'odierna architettura del dispositivo e che anzi in qualche modo essa le limiti.
In questo lavoro inizialmente ci si è concentrati sulla realizzazione di dispositivi MSSC, con cui si poter comparare le prestazioni di diverse architetture. In particolare si è provato a sostituire il classico Hole Transport Layer (HTL) (Spiro-oMETAD) con *Disolfuro di Molibdeno*(MoS_2), avente migliori proprietà di conduzione e minor costo.

Per la realizzazione del HTL di MoS_2, sono state provate due differenti architetture:

- Film uniforme formato da flakes interconnessi di MoS_2
- Flakes di MoS_2 dispersi in matrice isolante (PVP)

Attualmente, sempre con l'obbiettivo di sfruttare al massimo le proprietà di conduzione della Perovskite, diversi studi mirano all'eliminazione dell'HTL, in modo tale da ridurre la perdita di fotocorrente dovuta all'accoppiamento materiale attivo/HTL.

Chapter 1

Introduction

1.1 Evolution and Market of PV Technology

The first time, in which was adopted the word "photovoltaic" was in 1883, when the first working PV device was obtained with sandwiched selenium between two sheet of metal. However the idea of use the photovoltaic effect to produce electric energy, was not presented since the selenium was substituted with other materials. The modern era of photovoltaic started in 1954 when the researcher, studying the diode technology, accidentally discovered that *pn* junction generated a voltage when the room light were on. During the same year they produced a 6% efficient Si *pn* junction solar cell. From that point onwards, thanks also the growing potential space applications, there was great interest by governments to improve the efficiency of this technology. In this scenario, the performance of Si technology increased about 30% and also began to born new class of photovoltaic cells, like CdTe and GaAs eterojunction. At the end of '60 years the available photovoltaic technologies, offered efficiencies upper 12%, but because of their high manufacturing costs, they were used only for space applications. The turning point was in 1973 with the first World Oil Embargo, instituted by the Persian Gulf oil producers. This highlighted the structural dependence of the industrialized world by fossil combustibles, which induced many governments to start programs to encourage renewable energy, especially solar energy. In the 1980s were born other technology like polycrystalline-Si and amorphous-Si having minor performances but with a cheaper manufacturing process costs than the classic single crystal-Si, which dominates the market today. Together with improvement of technology, the subsidy programs, such as feed-in tariffs adopted by many countries to make PV cost competitive with the fossil energy generation, have play a fundamental role in enhance of production to reduce costs. Thanks this, in the last decade the production of solar cell has

grown by over 50% by year and in the 2011 the cumulative installed capacity reached 69GW[8].

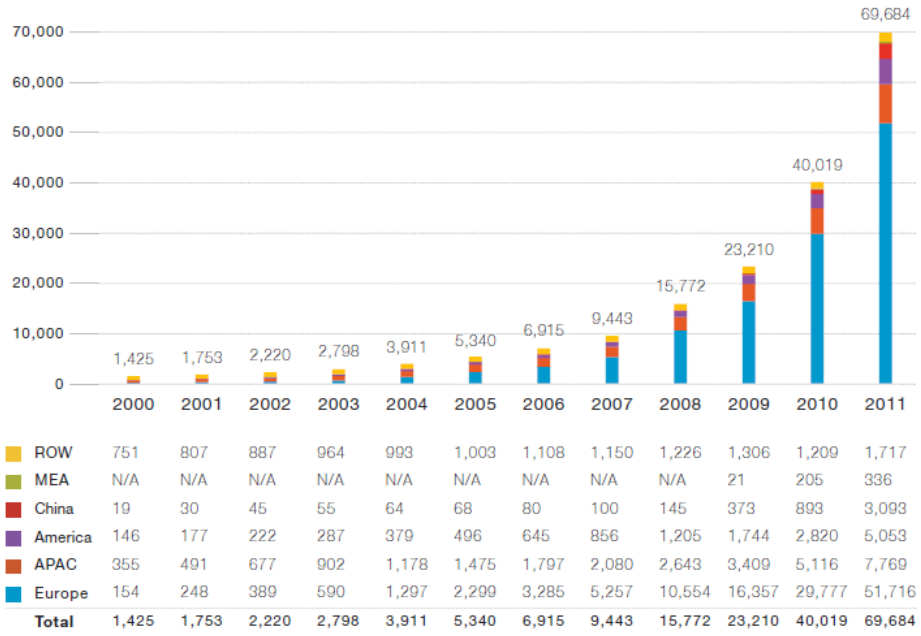

Figure 1.1: Global cumulative installed capacity in GW[1]

Despite the exponential growth of the installed PV capacity, occurred in the last years, the total contribution of solar PV to renewable electricity supply is still small, averaging 2% of the total electricity in UE, which is only 0.5% of globally electricity demand[8] Today, the PV technologies most diffused in the market are those based on crystalline silicon, in particular as is shown in Figure1.2,which produce more than the 85% of the overall photovoltaic production.

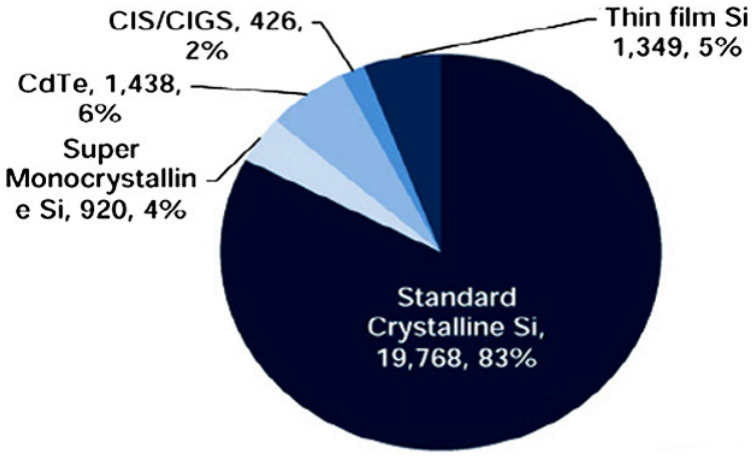

Figure 1.2: Photovoltaic production at 2010 in MW-dc. The total area is 23.889MW

This predominance was initially favoured by two factor, one technological and the one economic. Infact the advanced silicon technology used in microelectronics industry was quickly adapted in PV manufactury. Furthermore was easy to procure material and equipment at reasonable price. This situation was maintained thanks to the good performance of this technology at relative more competitive prices than other efficient technologies, having prohibitive costs in large-scale market. However the effective high price of crystalline solar cell, driven the research to look for new technologies to reduce the material cost for their production.

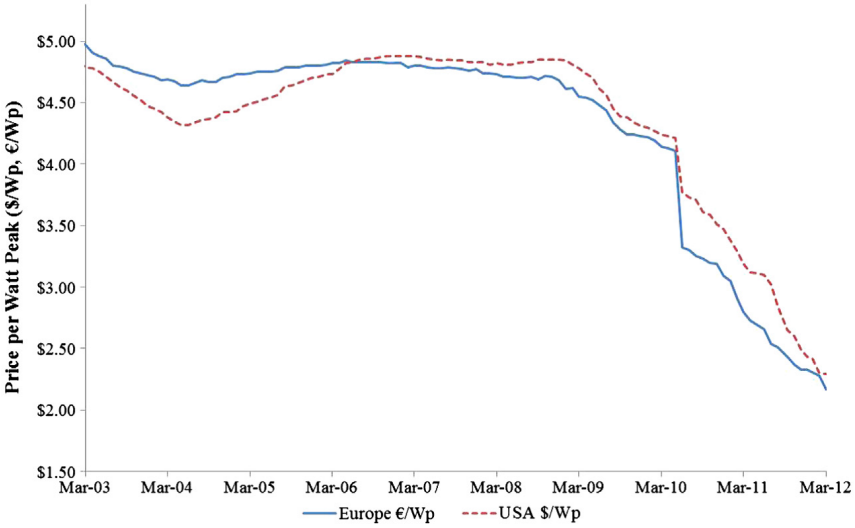

Figure 1.3: Curves rappresenting PV module retail price index 2003–2012, (€/Wp and \$/Wp). The cost is related to Watts of peak (Wp), which is the power that the module would deliver to a perfectly matched load, when it is illuminated with $1\frac{Kw}{m^2}$ of luminous power at fixed temperature of $25C°$ and in 1.5AM spectrum conditions.
Note: The presented curves are the average retail prices in Europe and the USA based on a monthly online survey. They encompass a wide range of module prices, depending to the used technology (with thin film modules generally cheaper than c-Si), the module model and manufacturer, its quality, as well as the country in which the product is purchased.
For example, in March 2012 the average retail module prices were respectively 2.29\$/Wp in USA and 2.17€/Wp in Europe, but the lowest retail price for a crystalline silicon solar module was 1.1\$/Wp(0.81€/Wp) and the lowest thin film module price was 0.84\$/Wp(0.62€/Wp)[8].

1.2 Overview On PV Technologies

As said in the previous chapter, numerous efforts have been made to improve the PV technology and to promote its diffusion in the great market. In this chapter will be shown the principal technologies which today are aviable in the market or still under investigation. A brief overview of PV technologies adopting different kinds of material is given by the following scheme in Figure1.4.

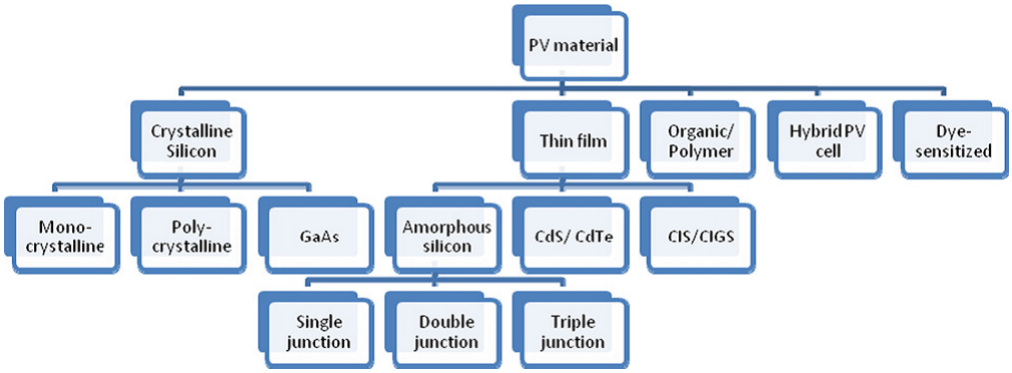

Figure 1.4: PV technologies chart

Starting from left we find the most diffuse PV technologies based on *crystal silicon*, in which *singlecrystal Si* and *multycrystal Si* are the most important exponents. They show high efficiency, about 28% in laboratory, which decrease to 17% in large area production. Multycrystal-Si is an alternative, which avoids the onerous growing crystal process required for single crystal-Si. Clearly it shows lower efficiency but at a more reasonable price.

The class of *thin film technology*, was born to reduce the manufacturing costs using less material. Infact this kind of solar cells, made with this technology, are very thin (about 35-260nm). The *amorphous silicon* is a very relevant material in this kind of technology, respect to other materials, such as *CdS/CdTe* and *CIS/CIGS*, which have environmental contraindication or adopt rare element as Te. The amorphous silicon is interesting, not only for its absence of environmental and availability problems, but also for its relatively inexpensive growing crystals technology. In the case of CdS/CdTe and CIS/CIGS the efficiency are higher(about 15%) but on the other hand they require more onerous process. The technology having highest efficiency(over 40%) are the *multijunction solar cells* fabricated from III-V semiconductors , which have several characteristic that made them suitable for application in solar cells. A wide selection of these materials is available with direct band gap,inducing high absorption coefficient, from 1 to 2eV, which is the range of interest for solar cells application. The most important semiconductor alloy are *GaAs* with a band gap of 1.42eV, and

$Ga_{0.5}In_{0.5}P$ with a band gap of 1.85eV. Despite their high manufacturing costs these cells, thanks several characteristic as radiation resistance and better thermal property than silicon, are largely used in specialized sector in which the extra costs are less important,such as space sector or industrial power production using solar concentrators.
More recent technologies as *organic solar cells*, use polymers as active material. With this kind of solar cells, the research community are working to reduce at the minimum the manufacturing costs, thanks to different solution processes, such as blade coating, screen printing and sprying. These allow the utilizazion of unconventional substrate as plastic, which is very interesting for new applications. In the last years the research is moving to other technologies also called *third generation PV*, in which the characteristics, as morphology and electronic properties, are manipulated by the using of nanoscale components, like in the case of *Nanotube*,*Quantum Dot* and *Hot Carrier* solar cells.

Recently particular attention has been focused on a very promising technology:*Dye Sensitized Solar Cell*(DSSC), which has reported higher efficiency (about 16% in laboratory) than amorphous-Si. In specific, as shown in Figure1.5, the great leap forward has been done with DSSC based on *Organo-Lead Perovskite* . Very similar to the DSSC and descending from it, is the *Meso Superstructure Solar Cell*(MSSC), whose structure and operating will be explained up ahead.

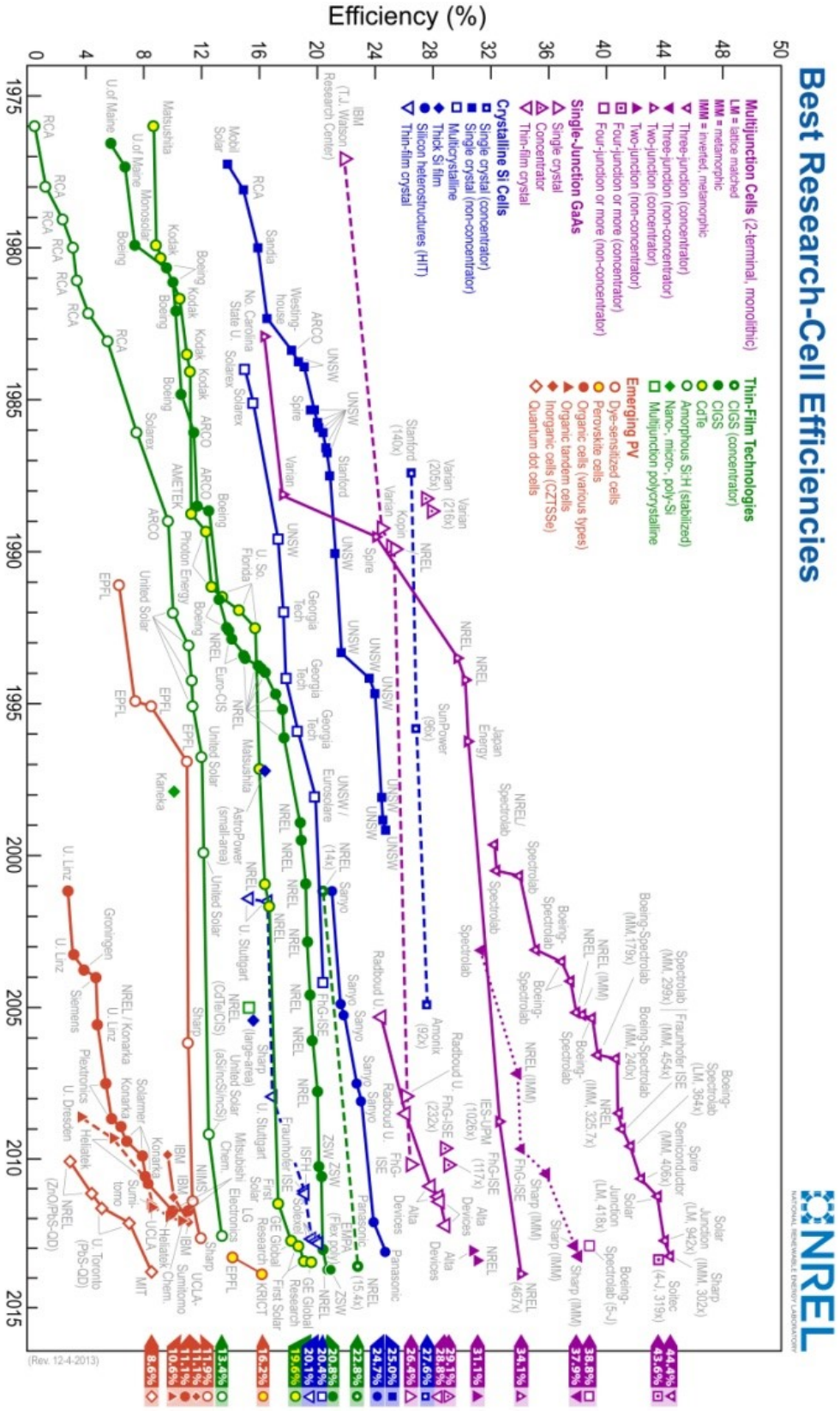

Figure 1.5: efficiency evolution of PV technologies, publishied by National Renowable Energy Laboratory

1.3 Theoretical Background

1.3.1 Ideal Solar Cell

Every solar cell is characterized by its *Short Circuit photocurrent*(I_{sc}) and its *Open Circuit voltage*(V_{oc}). The first is the maximum photocurrent due to the direct connection of the opposite contacts without any load between them, the second is maximum potential applied (due to an opportune load) to cell for which the generated photocurrent is perfectly balanced by *Dark current*(I_{dark}). The photovoltaic effect, so generation of photocurrent, occurs when a pair of electron-hole is generated by absorption of a photon and then the charges are separated and are collected forward respectively contact. Since the short circuit photocurrent density J_{sc}, is related to incident spectrum (b_s), through the as called *quantum efficiency*(QE). The QE is the probability that an incident photon of energy E, delivers one electron to the external circuit. The relation is given to

$$J_{sc} = q \int b_s QE dE$$

In which for standard conditions the used incident spectrum, is obtained to emission spectrum of black body at 6000 C°(sun) to which are subtracted the absorption due to atmosphere gas. The shape of spectrum changes depending to sunlight's path through the atmosphere, so depending to latitude.

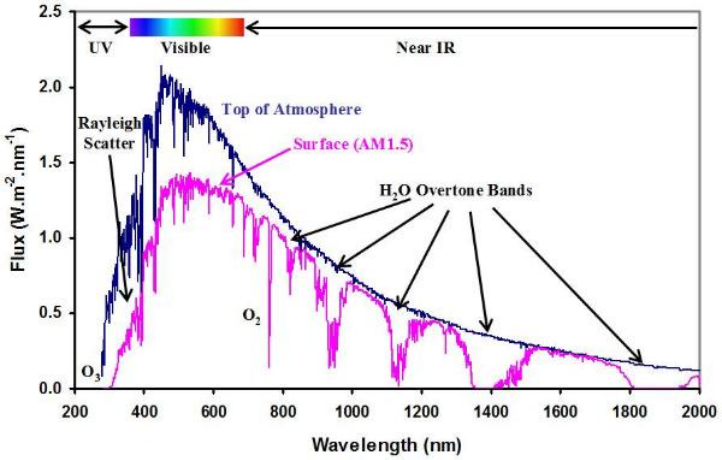

Figure 1.6: In blue solar spectrum at the top of atmophere(AirMass 0), while in violet solar spectrum at Earth's surface for temperate zones(AirMass 1.5)(http://venturaphotonics.com/).

In ideal case the Dark current, is the current absorbed by a device when is applied a direct potential between the two contacts, that in the case of a solar

cell it is due to supplied load.

$$J_{dark} = J_o(e^{qV/KbT} - 1)$$

where Jo is a constant, Kb is Boltzmann's constant and T is temperature in Kelvin degrees. As will be explain up ahead, in real devices at this term, is added a certain quantities due to presence of non-ideality, which induce more recombination of the photo generated charges. Therefore, the net extracted photocurrent in ideal devices is given to

$$J_{ph} = J_{sc} - J_{dark} = J_{sc} - J_o(e^{qV/KbT} - 1)$$

In first approximation, the operating of a ideal solar cell can be describe with equivalent electric circuit showed in Figure1.7. Where the Jsc is depicted by an ideal current generator and Jdark is emulated by an antiparallel diode.

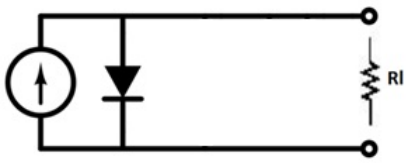

Figure 1.7: Equivalent electric circuit for an ideal solar cell.

The ideal solar cell should supplies a steady current (J_{sc}) independently to powered load, up to its theoretical maximum potential (when antiparallel diode turn on), given to

$$V_{oc} = E_g/q$$

where E_g is the band gap of active layer and q is electron's charge. The electrical power delivered in every operating point is given by $P = JV$, whose maximum (P_{max}) occurs at specific potential V_m and current I_m. In ideal case these values correspond to V_{oc} and I_{sc}. The *power conversion efficiency*(η) is the fraction of max delivered electrical power (P_{max}) related to the electromagnetic power coming to the incident light (P_{sun}), so given to

$$\eta = P_{max}/P_{sun}$$

1.3.2 Real Solar Cell

As said in the previous section, in the case of real devices exist further recombination channel due to presence of trap states, defects or imperfect interfaces. This causes an enhancement of lost current, which is efficaciously described by addition of two resistances in equivalent electrical circuit; *series resistance* (R_s) and *shant resistance* (R_{sh}).

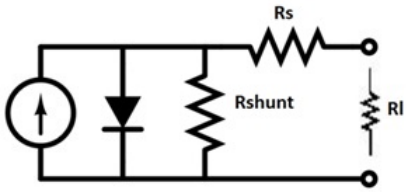

Figure 1.8: Equivalent electric circuit for a real solar cell, in which are added *series resistance* (R_s) and *shant resistance* (R_{sh}).

In this configuration, R_s represents the met resistance by charges, to reach the collecting zone. The entity of Rs depending to charges's mobility in the crossed mediums and their thickness. Otherwise Rsh describes the quantity of charges that recombines before are collected. The entity of both Rs and Rsh, depending to characteristics of crossed layer, as purity or intrinsic electronic properties. The presence of these resistances, weigh in different way on leakage of current respect to ideal J-V characteristic. In Figure1.9 are reported the shape changes due to R_s and R_{sh}

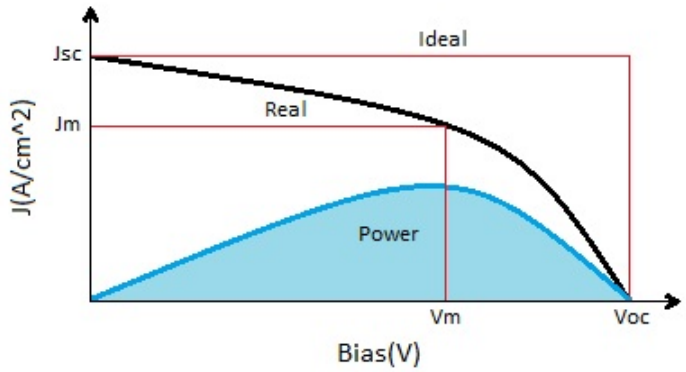

Figure 1.9: J-V curve of a real device and its generated power depending on applied load. The operating point with the maxima power is identified by pair (J_m;V_m).

The effect, due to deformation of J-V curve, on efficiency is described by a coefficient called *Filling Factor*, given to

$$FF = V_m I_m / V_{oc} I_{sc}$$

FF represents the ratio between squares depicted in Figure1.9, whose vertexes are identified by operating points delivering the max electric power. The greatest square are related to ideal case and the other is relateted to real case. Therefore for a real device the maximum efficiency is reduced by FF

$$\eta = J_{sc} V_{oc} FF / P_{sun}$$

1.4 Aims and Motivations of the Thesis

This thesis is structured in two sections:

- In the first part, the aim is to try to reproduce the state-of-art(16% of efficiency) of Meso-Superstructured Solar Cells using Organo-Lead Perovskite as photoactive material. Therefore, at this stage the task was to realize and to characterize operating devices.

- In the second part, the aim is to try to improve the performances of MSSC devices by substituting the *Spiro-oMETAD*, a molecular hole trasporter with *Molybdenum Disulfide*(MoS_2), maintaining the fabrication method solution-processed.
  As will be better explained in following chapters, Spiro-oMETAD is an optimized semiconductor molecule used as hole transporter in standard MSSC structure. However its molecular nature sets relatively low mobility of charges, so it determines very high resistance respect with other semiconductors. Furthermore, despite the slim consumption of Spiro-oMETAD for realization of a solar cell, it is the material which mainly weighs on the stability and cost of the overall device.
  The idea is to replace the Spiro with cheaper Molybdenum Disulfide which also has better conductive properties, in order to reduce the loss of photocurrent during the charge collection process.
  In particular, considering the equivalent electrical circuit, the desired effect is that to reduce the Rs maintaining unchanged the value of Rsh. It is important to highlight that the value of Rsh, rappresenting the entity of recombination, is not depending only by intrinsic properties of charge transporter, but also by the quality of the interface between the latter and photoactive material. In order to maintain solution-processing have been chosen the adoption of MoS_2 nano-flakes dissolved in solution, whose

properties will be presented in 3th chapter. While the implemented structures for the use of MoS_2 as hole transport layer, will be presented in 2th chapter.

Chapter 2

Structure and Fuctioning From DSSC to MSSC

2.1 Generic Structure Of DSSC and MSSC

At first sight,the generic structures for DSSC and MSSC technologies are identical. This because they show the same sequence of layer, but having different features of band structure of nanoporous structured material, which leads substantial changes in the operational mechanisms of the device.
In particular, as it will be presented later, for DSSC is adopted a semiconductor oxide, while for MSSC is adopted an insulator as mesoporous scaffold. As shown in Figure2.1 starting from the top layer, are located:

- SUBSTRATE: it gives mechanical resistence to the device and it acts like support during the fabbrication. Actually,in the majority of research activities is still used glass substrate, though promising results have been obtained with PET substrate [10]

- TRASPARENT CONTACT : In order to ensure the light transmittion through the device, the upper contact must be transparent to radiation belongs to the absorbption spectrum of active layer. Tipically are used *fluorine-doped tin oxide* (FTO) or *indium-doped tin oxide* (ITO).

- ELECTRON TRANSPORTING LAYER: *electron transporting layer* is an oxide semiconductor, having a band alignment to favour the transfer of electrons and at the same time block the holes coming from photogeneration.

- NANOPOROUS STRUCTURED MATERIAL: Layer with nanoscale morfology having different functions depending from its nature. In case of DSSC it is a semiconductor and it actively participates to charge separetion

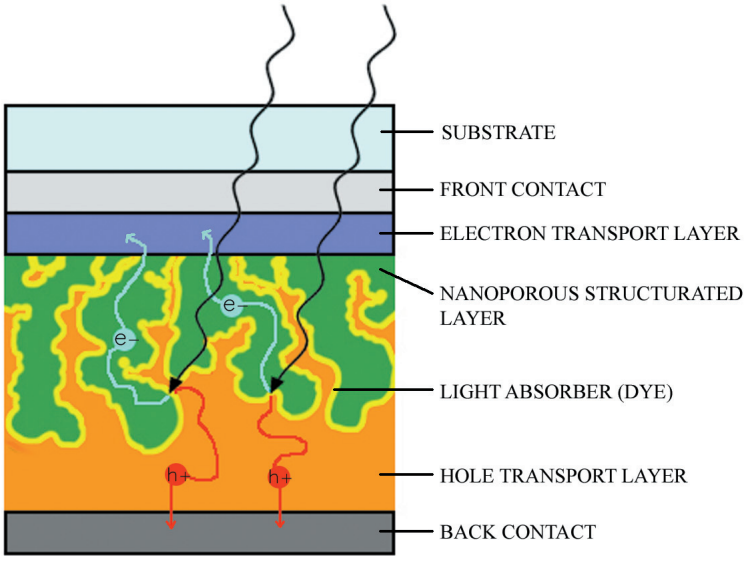

Figure 2.1: Generic structure of DSSC

phase. While in MSSC, inwhich mesoporous material is a insulator, it acts only like scaffold, ensuring the optimized morfology of the photoactive material(absorber).

- LIGHT ABSORBING MATERIAL: The material that creates exiton or free carriers following to the absorption of photons. There are three different categories of light absorber for DSSC technology: quantum dot, organic or organo-metal complexes.
  Organic sentitizers often limits light harvesting ability, because to their low absorption coefficient and narrow absorption.
  Quantum dots such as CdS, CdSe, PbS InP and InAs, although having intense light absorption, however not allowed high performance bacause significant losses in light utilization and charge separation at semiconductor-sentitizer interface. Since many years the research activity in field of DSSC technology, was foucused to find optimal absorber through the study on many different materials. In the last 12 months the attention has been focused on *organo-metal halide perovskite* due to its excellent light-harvesting characteristics. [5]

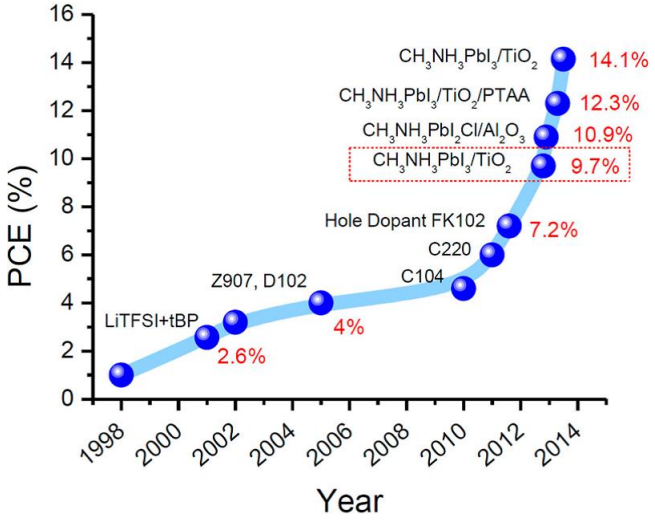

Figure 2.2: Improvement of PCE (power conversion efficiecy) in DSSC technology using different dyes

- HOLE TRANSPORTING LAYER: Likewise as electron transport layer, the *hole transporting layer* can be an oxide semiconductor or organic semiconductor, having a band alignment in order to perform specular activity respect to electron tranport layer.

- CONTACT: it is always a metal because it ensures an optimal ohmic contact, usually is adopted gold or silver .

2.2 Opereting DSSC

Dye sensitized Solar Cells,as the name suggests, use a photoactive material (dye) with broad absorption spectrum, in order to sensitize at the visible light an oxide semiconductor, that in conventional cell is *electron transport layer*](ETL). The reason because the photoactive material is applied just like pigment, is due to the fact that, tipically the absorbers adopted in this technology have high extinction coefficient but bad conduction properties. When a photon is absorbed by the dye, an exiton is generated and it propagates just untill the interface dye/ETL. At this point the exiton is separated into an electron and a hole, which are collected respectively forward ETL and generic Hole Transport Material(HTM). In this way the transport of charge is immediatly entrusted to ETL and HTM, giveing to the dye only the task of photogeneration. Since the harvest of the light take place only in a monolayer of the sentitizer material and nanoporous structered is used, in order to increase active area dye/ETL. If on the one hand mesoporous layer improves the light harvesting, with consequent increas of Jsc,

on the other hand it affects negatively the Voc respect to that achived with planar heterojunction[12]. Furthermore the utilization of nanostructured ETL gives rise problem about the realization of continuous and uniform interface from dye and HTM. In this sense have been made many studies, whose common target was find optimal HTM which guaranteed both good p-type conduction and pore filling of mesostructure[11][9].

In order to incentives the dissociation of the exciton in free charges, is necessary that the sistem composed by ETL/DYE/HTM has a profile of energy levels such as the one showed in Figure2.3.

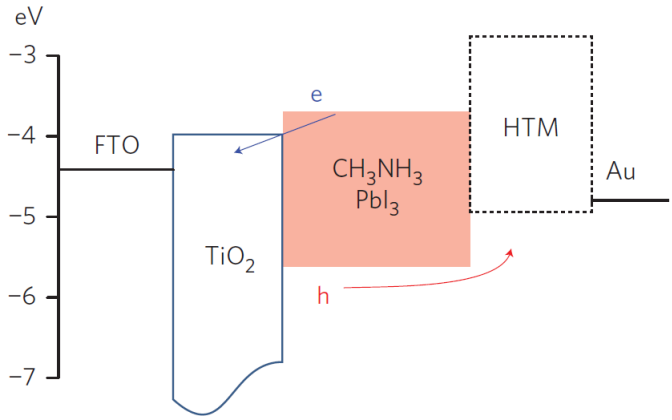

Figure 2.3: Schematic energy diagram of a classic DSSC using mesoporous TiO2 ETL, Organo-Lead Perovskite compound ((CH3NH3)PbI3) as active layer and generic Hole Transport Material(HTM)

Here is easy to see that the electrons in dye are energetically favored to cross into TiO2, while meet a barrier to flow torward HTL, viceversa for holes. In this way, is avoided the ricombination and is promoted the exstraction of a net current from device under illumination.

Initially the DSSC consisted of a mesoporous n-type (TiO_2) electrode sensitized by a dye and placed in a liquid electrolyte(tipically I^-/I_3^- redox couple) which acted as HTM. Since the dyes forms only a monolayer ,so the mesoporous presented must be $10-15\mu m$ thick to ensure complete light absorbing. As say before, the research worked to find alternative semincunducting sentitizers(as QD) in order to reduce the mesoporous TiO_2 layer thickness. In 2009 was made the first perovskite sentitized solar cell utilizing $CH_3NH_3PbI_3$ and $CH_3NH_3PbBr_3$ as absorber on TiO_2 mesoporous immersed in halide electrolytes, showed significative efficiency that rapidly was enhanced until 6.5%. Further breakthrough in both efficiency and stability was achieved in 2012 thanks utilizations of solid –state hole transporter (which called Hole Transport Layer(HTL)) $2,2',7,7'-tetrakis(N,N-p-dimethoxy-phenylamino)-9,9'-$

spirobifluorene(spiro-OMeTAD), with $CH_3NH_3PbI_3$ and $CH_3NH_3PbI_{3-X}Clx$ light absorbers (efficiency of 9.7%). In Figure2.4 are reported the structure and a SEM cross-section of a real device.

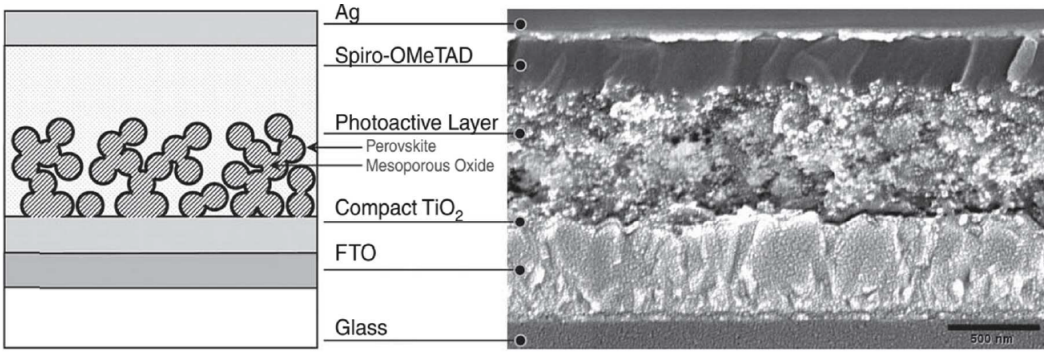

Figure 2.4: Schematic illustrating mesoporous perovskite solar cells[16]

From then on, there was great attention on DSSC based on Pervoskite sentitizer, which moves the research to try new architecture with a great variety of configuration, depositions protocols and materials, like in the case of MSSC.

2.3 Opereting of MSSC

The *Meso-Superstructured Solar Cell* is a technology deriving from DSSC using absorber with good conductivity as in the case of cells based to *Organo-Metal Perovskite*. Indeed several type of pervskite compounds have a mobilities comparable to amorphous silicon [2] and electron-hole diffusion length over $1\mu m$ [14]. These conditions have allowed to test different structures, in which the dye participates, not only to photogeneration, but also transporting charges. This is obteined by sostitution of semiconductor (TiO_2) in DSSC with insulant (Al_2O_3) in MSSC, so that mesoporous layer does not take part to any photovoltaics process's steps, but only like a mesoscale *scaffold* upon which the dye is structured.

Tests have demostrated that Al_2O_3 cells shows a V_{oc} grater than TiO_2 cells, with comparable J_{sc} and slightly lower fill factor.[7]. These results are justified by absence of, so called *chemical capacitance* due to entrapment of electrons by interband states of TiO_2. Further the good performance of these devices have highlighted that the perovskite within the mesoporous layer is continuous, in contrast to previous studies which had considered them as isolated quantum dots. Recently studies indicated that $CH_3NH_3PbI_3$ exists as two components within the mesoporous TiO_2, one component with medium range of crystalline order (30 atom %) and another with only local structural coherence (70 atom

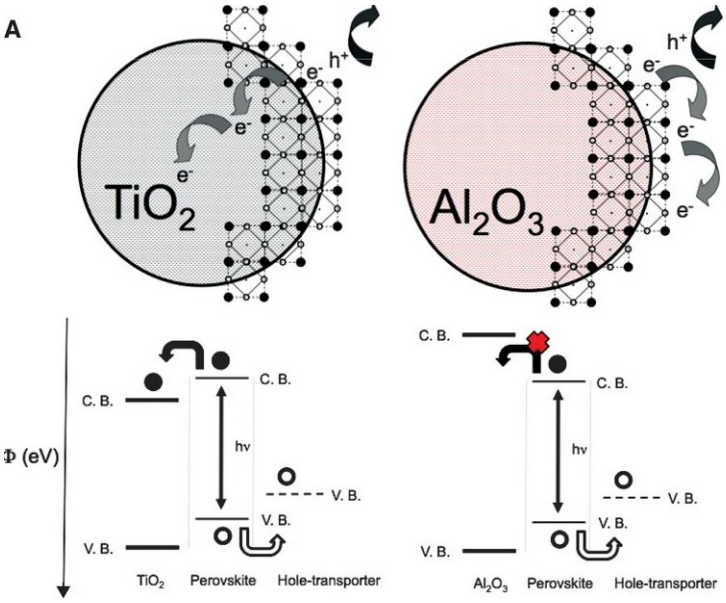

Figure 2.5: Schematic illustrating the charge transfer and charge transport in a perovskite-sensitized TiO_2 solar cell (left) and noninjecting Al_2O_3-based solar cell (right); a representation of the energy landscape is shown below, with electrons shown as solid circles and holes as open circles.

%).

The use of Organo-Lead Pervoskite, both in MSSC and DSSC, has determinated a drastic redesign the concept of absorber like just a dye. Indeed thanks to good transport property of the Perovskite, for an optimal collect of charges is no more necessary that HTL penetrates into mesostructure, but is sufficient that it be a thin layer acting as mere *electron blocking layer* between dye and back contact

The validation of electron transporting nature of the perovskite, is come by*pseudo-thin film* MSSC having very thin (80nm) Al_2O_3 scaffold. As shown the cross section inFigure2.6 there are a thick layer of Perovskite acting as absorber and charge transporter, which produced Jsc of $16.9 + -1.9 \frac{mA}{cm^2}$[16]. The ambipolar nature of Perovskite allows its using in ETL- free configuration or in HTL-free configuration.

For these reasons it was taken in considerations the possibility to crate *thin film solar cell based on Perovskite* with planar configuration (FTO /compact TiO_2 / $CH_3NH_3PbI_{3-X}Clx$ / spiro-OMeTAD / Ag), which shown 1.8% of efficiency. This unsatisfying performance, are imputable to the difficulties associated to fabrication of pin-hole free thin films through solution based process.

However thanks to these characteristics, the Perovskite permits low leakage of photocurrent also having high thick. In particular,in the best performer of

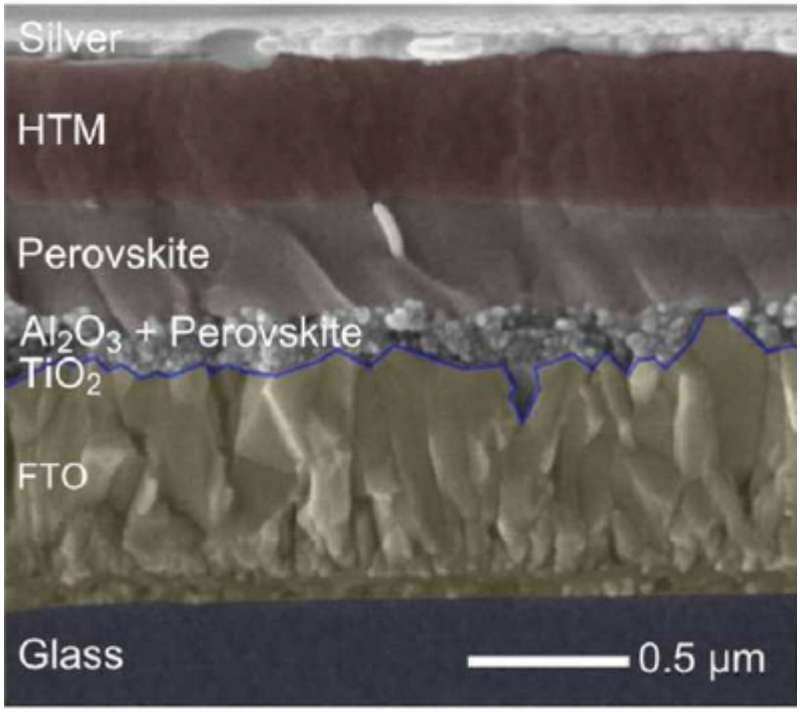

Figure 2.6: Cross-sectional SEM view of a "pseudo-thin film" architecture employing a thin Al2O3 mesoporous layer with a significantly thick perovskite film over it)[16]

MSSC structure, the perovskite layer comes out to mesoporous Al_2O_3 for several hundreds of nm, creating pillars which protude toward back contact (Figure2.7). In this way, is generated a dye/HTL interface that limits pore filling problem and reduces the average thickness of HTL, which is main responsible of series resistence of the device.

2.3.1 MSSC Using MoS2 As HTL

In order to obtain the optimal implementation of MoS_2 layer in solar cell's structure,two different kinds of devices have been tested. The difference between these two devices, is not only represented by the deposition modality, but also by the morphology and the operating of the MoS_2. The initial idea was to create a uniform film of interconnected flakes Figure2.8, which facilitated the flow of holes simply making available better conductive properties than *spiro-MeOTAD*. The main problem in implementing this structure was the high roughness of *Perovskite* layer (about 1μm) and very low concentration of flakes ($18\frac{mg}{l}$), impending the complete separation between active layer and back contact, so increasing the losses of photocurrent.

At a later stage, aided by the fact that was very uncertain the chances to create a uniform film with our concentration of MoS_2, a second structure was

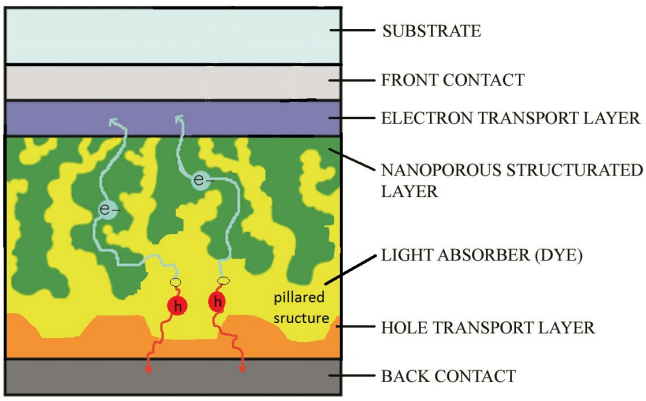

Figure 2.7: Structure of MSSC with pillared layer of Perovskite

developed using an insulating polymer(*Polyvinile-Butilacetate Pirrolidone*) as matrix for flakes. As it is easy to see in Figure2.9 representing in detail the MoS_2 layer, the idea is to create an insulator matrix, in which are dispersed flakes having random orientation. The thickness of matrix must be tuned in order to ensure that several single flakes can be able to cross its, from a side to the other. In this way the crossing flakes of MoS_2 act as preferential path for holes, ensuring at the same time insulation between active layer and back contact. The path for hole collecting is formed by single flakes to solve the problem of low concentration. Furthermore the use of a matrix allows a better coupling with extremely roughness of *Perovskite*. Moreover to more concrete possibility to realize an operating layer, this architecture offers low series resistance respect to uniform film, because to lacking of interfaces due to interconnected flakes, which characterized the first typology of devices.

As it will show in the following chapters, in order to obtain the optimum thick of matrix have been tested different concentration of polymer with different deposition condition allowing the correct viscosity of solution to favour random orientation of flakes.

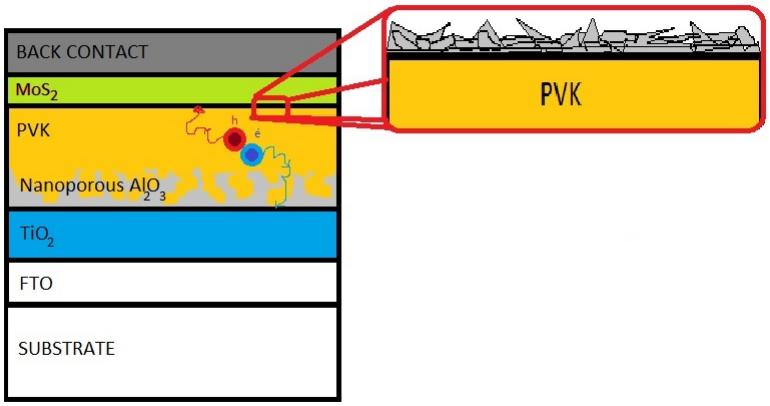

Figure 2.8: Architecture of MSSC using as HTL a film of interconnected flakes of MoS_2

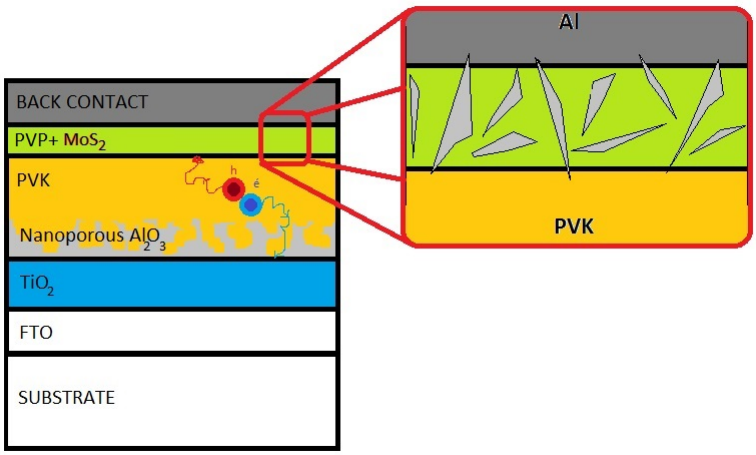

Figure 2.9: Architecture of MSSC using as HTL a matrix of PVP containing dispersed flakes of MoS_2

Chapter 3

Materials

3.1 Organo-Lead Halide Pervskite compound as sentitizer

3.1.1 Perovskite compounds

The *compounds Perovskite*, take their name from russian mineralogist Perovsky, who first charcterized the structure of a broad family of materials descrivible by this generic formula AMX_3; where A= cations (Ca,Mg,Cs,), B= metal cations (Ti,Pb,Sn..) and X= anions (O_2^-, Cl^-, I^-, Br^- etc). Between the beginnig of the eighties and the late nineties, the structure of this materials have been intensely studied for their many interesting properties and practical applications, such as colossal magnetoresistance, ferroelectricity, superconductivity, transport properties,etc. In the last two decades Perovskite compounds, have raised growing interest about their distinctive optical properties, which are related to their unique crystal structure. In Figure3.1 is showed the basic structure arrangend to a square cell of generic cations(A) containg MX6 octahedra, where M located at the centre and X lies in the corner. The MX_6 octahedra form an extended threedimensional (3D) network by all-cornerconnected type (Figure3.1), inside which is placed cations (A) balancing the charge of whole network.

The cubic shape of *basic structure* can be deformed following of different causes as: (i)off-center displacement of the M cations in the MX_6 octahedron,(ii)too small A cation at the cuboctahedral site, (iii) ordering of more than one kind of cations A or M and much more [3].

3.1.2 Organo-Metal Halide Perovskite((R-(CH2)nNH3)2PbX4)

The *Organo-Metal Halide Perovskite* is obteined when in a classical Perovskite compound, A is replaced by organic cations, which often, thanks to its reduced

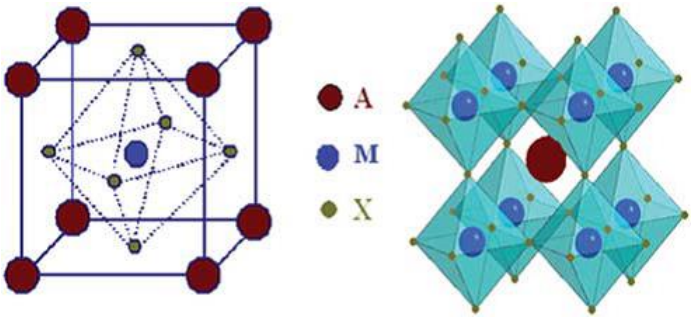

Figure 3.1: (a) Ball and stick model of the basic perovskite structure and (b) their extended network structure connected by the corner-shared octahedra.

size, is used methylammonium. In most hybrid composites the aggregation between organic-inorganic components occours randomly, causing a shortrange structural ordering. Otherwise Organo metal Perovskite show amazing self-assembling process determining long-range crystal, also by a fast spin-coating method. Considering the section of 3D network you can see that resulting 2D network, reported in Figure3.2 shows layered structure, in which the mono-layer inorganic perovskite slabs are sandwiched by the organic amine molecules. The organic molecules can be double layer (a) or single layer(b), depending on functional group R.

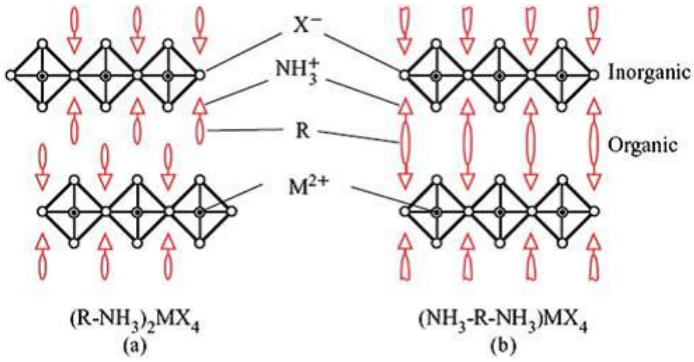

Figure 3.2: The basic structures of 2D organic–inorganic perovskite with bilayer (a) and single layer intercalated organic molecule

Another interesting characteristic of these hybrid compounds is the possibility of enhance the number (n) of inorganic layer, acting on stoichiometric ratio of the precursors or adding another small organic cation [3]. In structure which show a high n,it present a change from semiconductor to metallic behaviour, that confirm the possibility of use Perovskite compounds to obtain materials with good transport properties.

Many studies were made in order to understand the reasons for which the self-assembling occurs [15]. Although this is not know yet, it is hypothesized

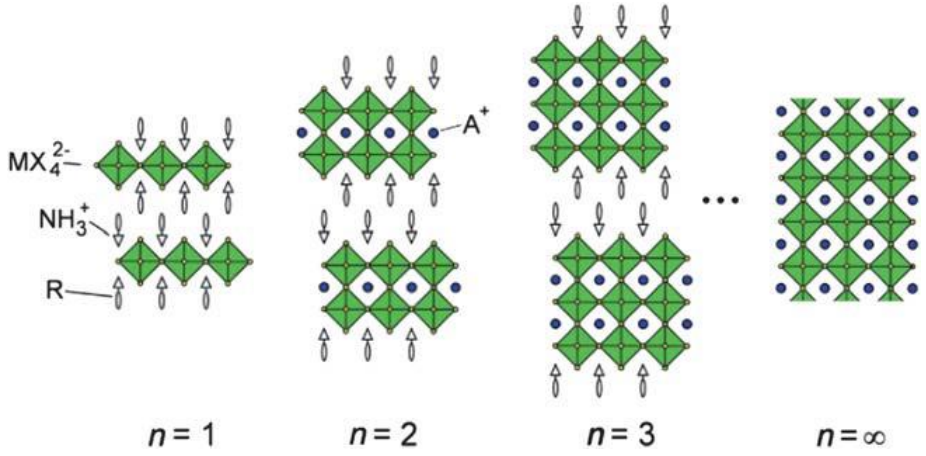

Figure 3.3: 2D network varing number of inorganic interlayers

that several driving forces of this process could be the predilection of inorganic ions to form the extended octahedral network by ionic bond and the trend of organic molecules to interact with inorganic sheet by Van Der Waals force.

Early studies on the electronic band structures have been made using ultraviolet photoelectron spectroscopy and first principles density functional theory (DFT)band calculation for room . These calculations for the 3-D $CH_3NH_3PbI_3$ crystal show that the valence band maxima is compounded by $Pb6p - I5p$ σ-antibonding orbital,while the conduction band minima consist of $Pb6p - I5s$ σ-antiboinding and $Pb6p - I5p$ π-antiboinding orbitals.

3.1.3 Photophysic in Peroviskite Compound

Although there was a rapid progress in organic-inorganic pervskite solar cell, the photophysical process driving the high performance of these material are unknown yet. In effect much of research work are focused on improve the device, leaving out the study of charge carrier dynamics. However, in order to investigate these aspects, several studies are been made on pervskite thin film through ultrafast optical spectroscopy (UOS) technique. Experiments of time –resolved PL shown for solution processed triiodide $CH_3NH_3PbI_3$ pervskite, diffusion lengths of 100nm both for holes that for electrons[16]. Much more interesting, is the case of mix halide $CH_3NH_3PbI_{3-x}Cl_x$ perovskite, in which both holes and electrons diffusion length are greater than $1\mu m$[**?**], although is not know if these results referring to free charges or exitons. These results have driven, in the last time, the choice of mix halile perovskite instead triiodide for the fabrication of devices. In fact from comparison between solution-processed thin-film planar heterojunction solar cells using the two differ absorbed, show

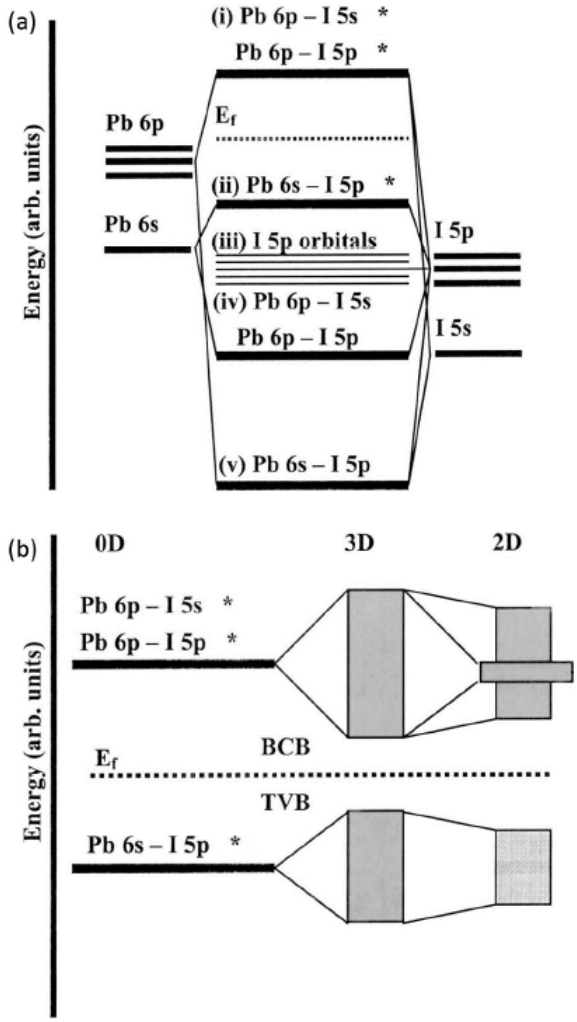

Figure 3.4: Electron states of (a)$[PbI_6]^{-4}$, (b)$CH_3NH_3PbI_3$(3-D) and (b) $(C_4H_9NH_3)_2PbI_4$ at the top the valence band and the bottom of conduction band[16]

significant differences in the performances. In Figure3.5are reported the J-V curve of the $CH_3NH_3PbI_{3-x}Cl_x$ planar heterojunction solar cell, which reach an efficiency of 12% with perovskite's thick of 500nm, in contrast with 4% of the best device based on $CH_3NH_3PbI_3$ and having active layer's thick of only 140nm[**?**].

Most recently, density functional theory (DFT) calculation made on $CH_3NH_3PbI_3$ bulk, have been highlighted low effective masses of both electron(me=0.23) and hole(mh=0.29). Furthermore high mobility of carrier have been measured in $CH_3NH_3PbI_3$ and $CH_3NH_3PbI_{3-x}Cl_x$, respectively of $8(\frac{cm^2}{Vs})$ and $11(\frac{cm^2}{Vs})$, which are extremely high for solution-processed perovskite. These results, establish further validation of long-range ambipolar charge transport property of these materials. In Figure3.6 are reported a schematic of the photophysical

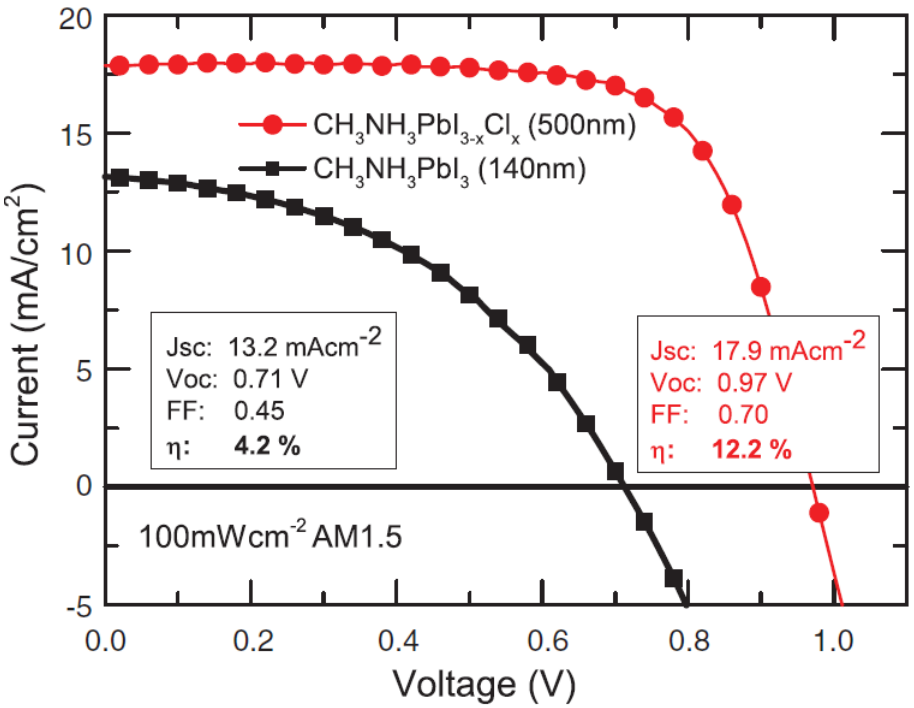

Figure 3.5: Current-Voltage curves for optimized planar heterojunction pervskite solar cell.$CH_3NH_3PbI_{3-x}Cl_x$ (red line, circle symbols) and $CH_3NH_3PbI_3$ (black line, square symbols) cell were both measured under $100mWcm^{-2}$ AM1.5 simulated sunlight.

process and the different losing channels which could occur after the photonexcitation. After absorption of a photon, a electron-hole pair is generated, and after their thermalization involve in the formation of highly delocalized *Wannier exitons*. These excitons show relatively low binding energies, in particular for $CH_3NH_3PbI_3$ have been demonstrated a binding energy(E_b) between 19meV and 50meV with a Bohr radius about r_b ≈30(AMSTRONG). Other perovskite compound, as $CH_3NH_3PbI_{3-x}Cl_x$ presents grater E_b indicating a more tightly bound nature of excitons, due to halogen substitution. As is noticeable inTable3.1, the same trend is shown decreasing in dimensionality (2D,1D and 0D) in which the growing quantum confinement effects produce much more bounded excitons (*Frenkel type*).

The low exciton binding energies in the range 20-100meV comparable with the room temperature thermal energies of $K_bT \approx 25meV$, demonstrates that fraction of excitons spontaneously dissociate in free charges. In this way, the excitons and free carriers coexist, so their dynamic populations continue to vary over their lifetime. Through the use of THz spectroscopy has been found that both the monomolecular (*germinate recombination* and *impurity-assisted re-*

Compound	Dimensioinality	E_b (meV)
$CH_3NH_3PbI_3$	3D	19 - 50
$CH_3NH_3PbBr_3$	3D	76 - 150
$CH_3NH_3PbI_{3-x}Cl_x$	3D	98
$(C_9H_{19}NH_3)PbI_4$	2D	≥ 330
$(NH_2C(I)=NH_2)_3PbI_5$	1D	≥ 410
$CH_3NH_3)_4PbI_62H_2O$	0D	545

Table 3.1: Exiton binding energies E_b of the 3-D $CH_3NH_3PbI_3$ and $CH_3NH_3PbBr_3$ perovskite and several selected low-dimension perovskites[16].

combination) and bimolecular charge carrier recombination rates are extremely low. Conversely, both *Auger recombination* and *Amplified Spontaneous Emission*(ASE) occur at higher pump excitations, although it is important to note that under solar light intensities (weak excitation) these losses channels would be strongly suppressed[16].

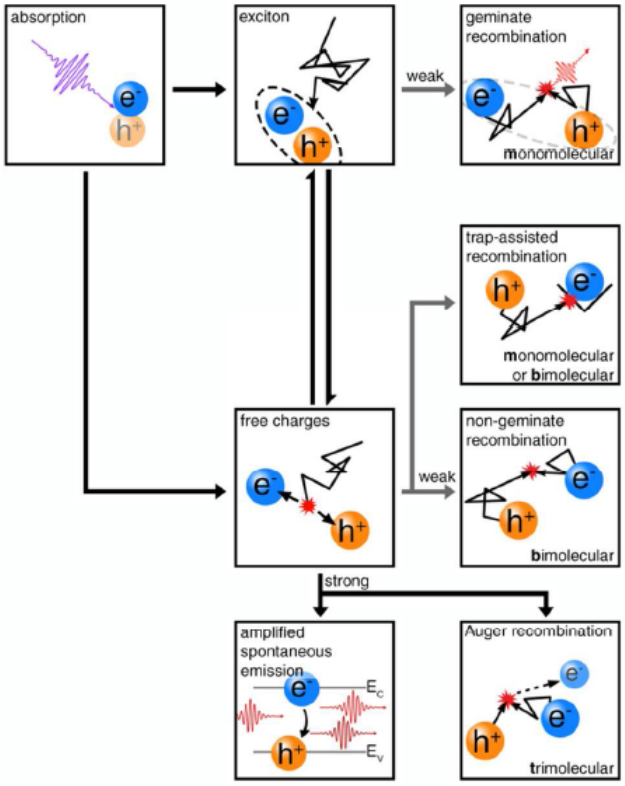

Figure 3.6: A schematic of the photophysical processes and loss mechanisms in perovskites following photoexcitation. Efficient paths (black lines) and suppressed paths (grey lines). Monomolecular recombination is charge carrier density independent, while bi-molecular and Auger recombination are charge carrier density dependent processes that would typically be present under strong photoexcitation. In fact, under even higher photoexcitation densities, amplified spontaneous emission (ASE) will outcompete Auger recombination. However, under solar light intensities (weak excitation), these latter processes will be strongly suppressed.[16]

3.2 Molybdenum Disulfide(MoS_2) in MSSC

3.2.1 Transition Metal Dichalconedies

Transint metal dichalcogenides (TMDC) are a class of materials with the formula MX_2, where M is a transition metal element from group IV (Zr, Ti and so on), group V (as V, Nb or Ta) or group VI(Mo, W and so on). These material show a layered structure X-M-X reported in Figure3.7, that presents strong ionic-covalent intralayer interactions and relatively weak Van Der Waals interactions between adjacent layers, which facilitates the formation of ultrathin crystal by exfoliation.

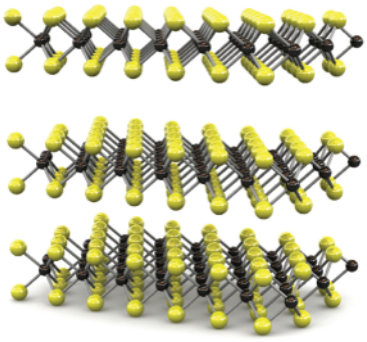

Figure 3.7: Three-dimensional schematic rappresentation of a tipical MX_2 structure, with the chalcogen atoms(X) in yellow and the metal atoms (M)in gray[13]

Although TMDCs are known since long time, the possibility of create 2D structure joint to interesting property of themselves and physical comprehension coming to graphene technology, have recently awaked a new scientific and engineering interest about them. Several semiconducting TMDs, among which the MoS_2, show a transition from indirect band gap, in bulk configuration, to a direct gap in monolayer, making them very interesting for electronic and optoelectronic applications. In particular in the case of MoS_2, as is showed in Figure3.8 the indirect band gap of 1.3eV in bulk material, changes in direct band gap of 1.8eV in a single –layer form[13][6]. This phenomena is due to quantum confinement and resulting change in hybridization between p_z orbitals on S atoms and d orbitals on Mo atoms. Density functional theory (DFT) calculation shows that the conduction band states at the K-point of Brillouin, are principally due to localized d orbitals of Mo atoms, which are localized in the middle of S-X-S layer sandwiches and for this reason relatively unaffected by interlayer coupling. Instead the γ-states are due to combinations of antibonding p_z-orbitals on the S atoms and the d on the Mo atoms, which suffer a strong interlayer coupling effect. Therefore lowering the number of layers, the K-states

remains substantially the same while γ-states change sanctioning the passage from indirect to direct material.

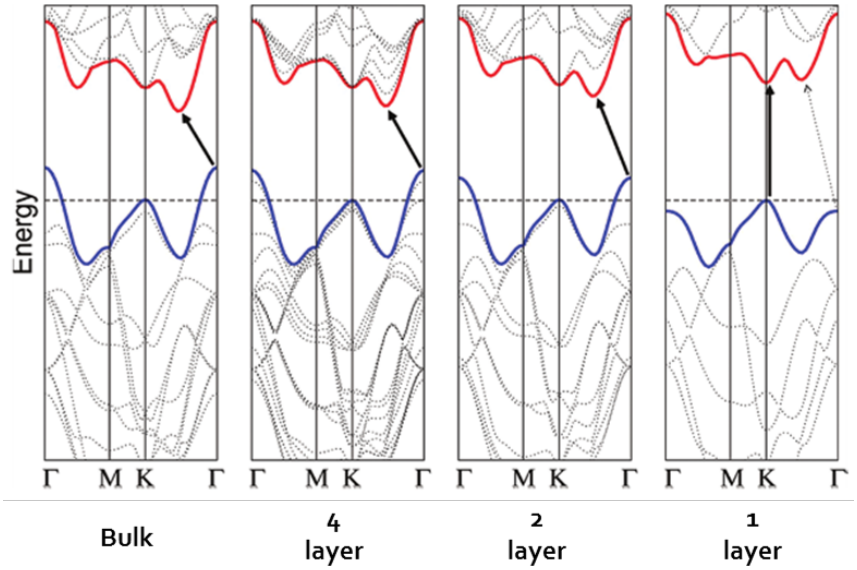

Figure 3.8: Band structure calculated by first-principles density functional theory(DFT)for bulk and monolayer MoS_2[13]

The interest toward this material about the MSSC, but more generally, about the photovoltaic technology is the possibility to obtain high quality of 2D structure created by mechanical-cleavage, which assuring the maintenance of solution-processing.

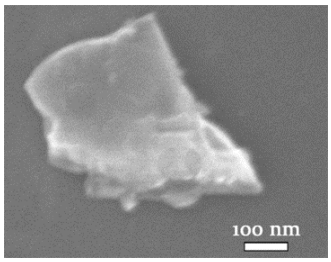

Figure 3.9: SEM image of a flake of MoS_2 long several hundreds of nanometers

3.2.2 MoS2 as HTL

The use of MoS_2 in MSSC technology should allowed conditions with higher electric characteristics then every other semiconductor polymer. In particular in the classical structure of MSSC the HTL is Spiro-OMeTAD, having a hole mobility on the order of $10^{-4}(\frac{cm^2}{Vs})$ in pristine form, which can reaches values higher of one order of size with doping of cations of Li^+ and Btp . However, the solution of doping reduce the stability Pervoskite, furthermore considering

its optimal conductions properties, the relatively low mobility in HTL produce an inevitable bottleneck effect about the current extraction, respect the potential performances. Therefore replace the Spiro-OMeTAD with MoS_2 having a mobility of carriers greater of five order of size, about $1.8x10^2(\frac{cm^2}{Vs})$, can reduces the series resistence (R_s) between active layer and back contact, during extraction of photogenerated charges. As touched in the previous section, the solution-processing of the devices can be preserved by adoption of MoS_2 2D nanostructure (*flakes*) dispersed in solution. In Figure3.10, the energy levels of every material composing the MSSC are reported, it is easy to see that MoS_2 is suitable as HTL. In fact, the configuration of MoS_2's energy levels, allows the injection of holes and the block of electrons coming to Perovskite.

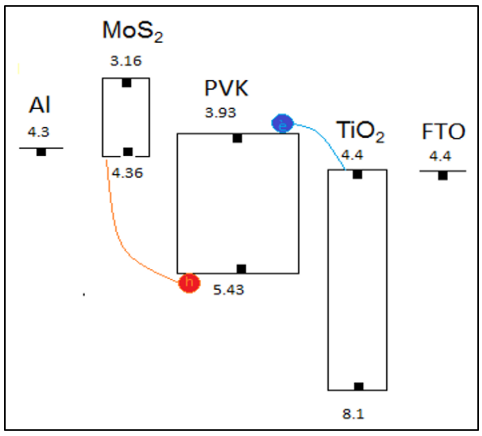

Figure 3.10: Energy levels of material composing MSSC with MoS_2 as HTL.You note that the energy levels in 2D structure ofen depending on many factors, as exfoliation method and annealing process. In this case are reported the energy levels of MoS_2 relative to a monolayer flakes [13][6]

Nevertheless the great band-offset existing between valence bands of Perovskite and MoS_2, it could be counter-productive due to the possibility of creation of a *Shottky barrier* for hole injenction. The band alignment deepening by electronic characteristics of the two participating material, so to know the possible formation and relative entity of the barrier, is needed to study in-depth the band of Perovskite.

Chapter 4

Methods

4.1 Fabrication of devices

For the discussion of material used and fabrication step, the specific structure of the device will be presented following the processing order, so from substrate to back contact. For both "classic" MSSC and "experimental" MSSC, using respectively *spiro-MeOTAD* and MoS_2 as HTL, have been required the same process step until deposition of light absorbing material.

- SUBSTRATE: *glass*
- TRANSPARENT CONTACT: *Flourine-doped Thin Oxide*
- ELECTRON TRANSPORTING LAYER: *compact TiO2*
- NANOPOROUS STRUCTURED MATERIAL: *nanoporous Al2O3*
- LIGHT ABSORBING MATERIAL: *(CH3NH3)PbI3-xClx (Organo Lead Mix Halide Perovskite)*
- HOLE TRANSPORTING LAYER: *spiro-MeOTAD*/MoS_2
- BACK CONTACT: *silver*

In order to enhance the statistics importance, every single device is composed by three different active areas called pixel.

4.1.1 Preparation of substrate

The fabrication starts with preparation of substrate on which will be process all other steps.
In our case the glass substrate, thick 3mm and already supplied with a covering

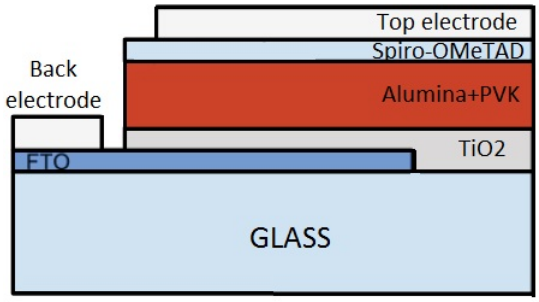

Figure 4.1: Schematic section of completed devices

layer of FTO thick 200nm. The fabrication batch is composed by eight devices, so a slide of substrate (glass+FTO) is previously cut and a preformed pattern is engraved on conductive side (FTO side). In order to avoid short circuit conditions during I-V tests, as show in Figure4.1, the opposite side to common contact, is deprived of FTO layer. This electrode pattern is obtained by chemical etching step with hydrochloric acid. Following the pattern, stripes of tape are placed where you want maintain FTO and for catalysing powder of metallic zinc is deposited on etching zones with subsequent addition of HCl solution (25%) by Pasteur pipette. After 30 seconds acid is removed by several rinses of distilled water and the tape is detached. Before perform any other process, a preliminary cleanness is made through two cycles, where in sequence, the slide is wiped by cotton swabs soaked, first with ACETONE and then with IPA. After drying by nitrogen gun the cleaning step is completed with plasma treatment for 10 minutes.

4.1.2 Deposition TiO_2 Compact Layer

The TiO_2 compact layer is performed by *spray deposition* of ethanol based solution containing the precursor *Titanium Disoproxide*. The needed solution for one slide (eight devices) is prepared in controlled nitrogen ambient, adding to $8ml$ of anhydrous ethanol 800μl of precursor. The substrate is placed under fumehood on programmable hot-plate, which is gradually heated until a temperature of $400C°$. At this point, the solution is put in a Venturi pipe connected with oxygen supply adjustable by hand. Under fumehood,as soon as the oxygen flux is strong enough to vaporized the solution the deposition can be started, beginning careful to uniformly distribute the flux on the slide and maintain always a distance from 20 to 30 centimetres. When the deposition is completed, the temperature of substrate is enhance until $500C°$ for 45 minutes so as to obtain the sintering process of TiO_2. After gradually cooling the slide

is fragmented in single devices, which are placed in $TiCl_4$ (2 molar) bath heated to $70C^\circ$ for 1 hour, in order to ensure the passivation of floating bonds at TiO_2 surface. After $TiCl_4$ treatment the devices are rinsed with distilled water and dried with nitrogen gun.

4.1.3 Deposition of Mesoporous Alumina

The deposition of mesoporous alumina is made by spin-coating of a IPA based solution obtained combining at 1:2 proportion Al_2O_3 with IPA and mix them by sonication process. The needed solution for one device is $100\mu l$ applied with peak speed of spin equal to $2500rpm$, which is reached in 1 sec and is maintained for 60 sec. When the spin-coat ends, the device is put on the hotplate at $150C^\circ$ for 20 minutes so as to totally evaporate the solvent.

4.1.4 Deposition of Organo-Lead Mix Halaide Perovskite

The deposition of Perovskite is performed in nitrogen ambient by spin-coating. The devices are put in controlled atmosphere ambient on hotplate at $100C^\circ$ for at least 10 minutes, in order to totally desorb the water. Subsequently the solution (40% Perovskite precursor in DMF) and substrate are heated and are maintained at $70C^\circ$. The spin-coat for every substrate is made depositing $50\mu l$ of solution at $2000rpm$ with $2000rpm/s$ ramp for 45 seconds. Time to time at the end of every run, the devices are placed on hotplate at $100C^\circ$ for 45 minutes in order to complete the Perovskite's crystallization. Process confirmed by change of substrate's colour from opaque gray to dark brown.

4.1.5 Deposition of Spiro-OMetad

As for Perovskite layer also the deposition of spiro-MeOTAD is performed in nitrogen ambient by spin-coating technique. The solution is obtained with following recipe: For every $100g$ of spiro-MeOTAD

- $0.926ml$ of chlorobenzene
- $82\mu l$ of solution containing additives (LiTFSI)

  Where for every $1g$ of LiTFSI

  - $11.61ml$ 1-butanolo
  - $1.36ml$ TBP

The spin-coat for every device is made depositing $70\mu l$ of solution at $2000rpm$ with $2000rpm/s$ ramp for 60 seconds.

4.1.6 Deposition of MoS2

As say in previous chapter the implementation of MoS_2 in MSSC has been carried out following two different architectures, as called *Film Layer* or *Matrix Layer*. For both kinds of devices the deposition of MoS_2 has been made by spin-coating of solution based water and ethanol, in which are dispersed the nano-flakes.

Solution of MoS2 flakes

For both kind of devices is used the same solution composed by:

- 55% of water
- 45% of ethanol
- nano-flakes(about $400nm$ of length) having a concentration of $18\frac{mg}{l}$.

As will see, the solvents presents in the solution have strongly influenced the choice of the polymer used to create the insulating matrix and its processing method. Indeed, about the insulating polymer, was necessary that it dissolved in water based solution. Furthermore more important, being the Pervskite soluble in water, was essential to reduce at the minimum the time of exposition of the Perovskite to the solution. For this reasons the spin-coat is effectuated to high speed of rotation, in order to accelerate the evaporation process. However for both method have been tested differ condition in spin-coating, as speed, acceleration and temperature of substrate.

Film Layer of MoS2 Flakes

The preliminary test on deposition of MoS_2 solution have been made just on glass covered by a thin layer of FTO and at later stage on glass covered by FTO and Pervovskite. It is important to highlight that in these samples, the Perviskite layer is deposited on flat layer(FTO) and not on meso-structure like in case of the devices, conditions that produces different morphology of Pervskite itself.
Below in Table4.1, are reported the condition test of spin-coating relating to two kinds of samples:

Substrate	Speed ($\frac{rpm}{s}$)	Acceleration ($\frac{rpm}{s^2}$)
FTO	1000	500
at	2000	500
T ambient	4000	1000
FTO	800	500
at	1000	500
$100C°$	2000	500
FTO+PVK flat	1000	500

Table 4.1: Preliminary tests of MoS_2 flakes on FTO and FTO+PVK flat.
* In this phase the speed have been kept at relative low values due to low viscosity of the solution, which tends to not hang on substrate.

MoS2 Flakes Dispersed in Insulating Matrix

Regarding the implementation of *Matrix Layer*, in order to not reduce further the low concentration of the flakes, the polymer is dissolved directly in MoS_2 solution. The polymer adopted is *Polyvinyle-Pyrrolidone*(PVP) which is soluble in MoS_2 solution. As for the case of *Film Layer* also for *Matrix Layer* have been made preliminary test on glass with FTO, with which to study the characteristics of the polymer film, as thick and roughness. In addition to the variation of the speed and the acceleration of the spin-coating process, it has been changed also the concentration of PVP present in solution. In this case, several spin-coating is effectuated on flight, in other words the solution has been deposited when the sample holder was already at maximum setted speed. This is for avoid the evaporation of solvents before that the polymer covers overall samples. Below are reported the experimented condition(Table4.2):

PVP Concentration($\frac{mg}{ml}$)	Speed ($\frac{rpm}{s}$)	Acceleration ($\frac{rpm}{s^2}$)
30	2000	500
	3500	1000
	6000	2000
30	2000	on flight
	3500	on flight
	6000	on flight
60	2000	on flight
	3500	on flight
	6000	on flight
100	2000	on flight
	3500	on flight
	6000	on flight

Table 4.2: Preliminary tests of MoS_2 flakes in insulating matrix of PVP varying: speed, acceleration and concentration of polymer

As will present in 5_{TH} chapter, the best depositing condition are show by spin-coating on flight. For this reason, the devices have been made by spin-coating on flight and with optimum PVP concentration ($100(\frac{mg}{ml})$).

4.1.7 Deposition of Back Contact(Ag)

The deposition of back contact is obtained by evaporation of Ag. Depending on kind of HTM adopted the sequences before evaporation is slightly different.
For devices using MoS_2 there is not any preparative procedure, while for devices using *Spiro-OmeTAD* is needed to expose it to air for several hours in order to dope its and enhance its conductivity. The devices are placed and are fixed on a mask, which reproduces the pattern of three pixels. The mask is put in the vacuum chamber of the evaporator. When the pressure is enough low (about $2 \cdot 10^{-6}$) the evaporation can begun. In order to avoid to damage the devices the first $10nm$ of Ag must be evaporated at low rates($0.1/0.2\frac{nm}{s}$).

4.2 Characterization Techniques

In this section, I am going broadly to describe the techniques adopted for the characterization of the fabricated devices. During my all period of work, was necessary *Current-Voltage Measurement*, which is the most common technique used in study of photovoltaics cells, but also other measures as *Transient Photocurrent Measurement* have proved useful for rough investigation about hysterical behaviour shown by devices. Furthermore in the second experimental phase, whose aim was the substitution of Spiro-MeOTAD with MoS_2, there was the necessity to study in detail the characteristics of single layer. In particular,for this porpouse have been use *Spettrophotometer* for UV-VIS measure, *Profilometer* for inspect the thikness and roughness and *Scanning Electron Microscopy*(SEM) for morphology study of the different samples.

4.2.1 Current-Voltage Measurement

The J-V curve is the most common measurement used in order to inspect the performance of solar cells and from which is possible to obtain information on fundamental factors as Isc , Voc , efficiency and FF. The measure is realized, illuminating the device with a lamp radiating solar spectrum and gauging the photocurrent depending on an applied potential, which emulate the supplied load. Depending to aspect to be investigated the values of testing potential can change in different range.
Tipically the needed equipment for measure of J-V curve are composed by a solar

simulator for to manage the irradiation, a kitley needed for electrical measure and a personal computer necessary to record the data.

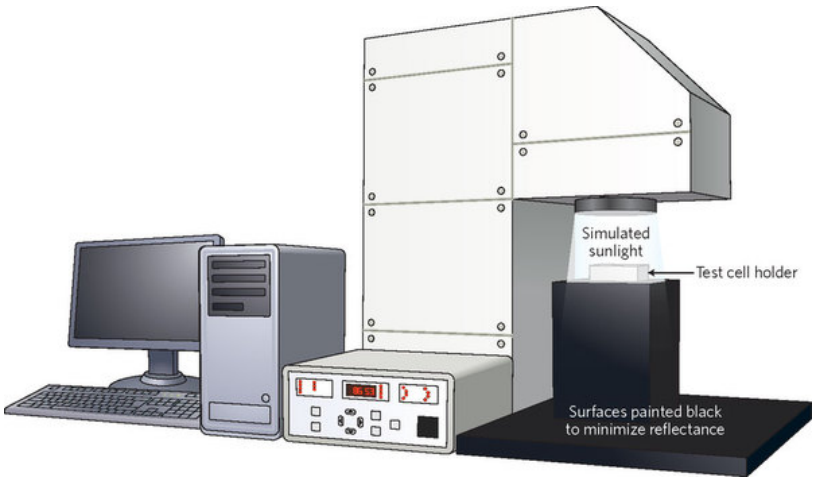

Figure 4.2: sperimental setup needed for J-V measurement. It is composed by a computer for storing of data, 1a kitlay to simulated the variable load and a solar simulator to emulate the sunlight.

Solar Simulator

The solar simulator is useful to supply suitable sunlight and to provide a controllable indoor test facility under laboratory condition.
For photovoltaic testing exist three standards that define solar simulator performance: *IEC 60904-9 Edition 2 (2007) (Photovoltaic Devices) , JIS C 8912-1998(Solar Simulators for Crystalline Solar Cells and Modules) and ASTM E 927-05 (2005) (Specification for Solar Simulation for Terrestrial PV).*
All standards define constraints about three factors:

- Spectral match:
  The standards define the spectral match of a solar simulator as a percentage of integrated intensity in six spectral rage for the more typical standard spectrums as AM0G, AM1G and AM1.5G. Any deviation from the specified percentages must then lie within a range that determines the class of the simulator. Below, in Table4.3 is reported the spectral contents for AM 1.5G spectrum.

- Spatial uniformity of irradiance:
  In order to avoid significant errors in measured cell efficiency, is needed that the irradiance has sufficient spatial uniformity. For this, every solar simulator has a working distance range in which is ensured the constraint on spatial uniformity.

Spectral Range (nm)	Total Irradiance Range (%)	Ideal (%)
400 - 500	13.9 - 23.1	18.5
500 - 600	15.1 - 25.1	20.1
600 - 700	13.7 - 22.9	18.3
700 - 800	11.1 - 18.5	14.8
800 - 900	9.2 - 15.3	12.2
900 - 1100	12.1 - 20.1	16.1

Table 4.3: Ideal spectral match definited by IEC standards for AM 1.5G

- Temporal stability:
  It requires that the output light be stable over time in order to ensure that the lamp fluctuations do not distort the measurement of solar cell efficiency.

Each factor, depending on respected constrains, is classified in one of three classes A,B or C. In Table4.4 are reported the limits, for each factors, defined by *IEC 60904-9 standard*

Classifications	Spectral match (each spectral intervals)	Irradiance spatial non-uniformity (%)	Temporal instability (%)
class A	0.75 - 1.25	2	2
class B	0.6 - 1.4	5	5
class C	0.4 - 2.0	10	10

Table 4.4: Solar simulator classification definited by IEC standard

Set-up Measurement

The solar simulator used for measure is *Oriel Sol3A* (class AAA) having ozone-free xenon short arc lamp, on which is displaced an Air Mass 1.5 G filter, all manage by a kitlay connected to PC. Both classical MSSC that MSSC with Mos_2, are been tested using two different settings:

- *Normal setting*, that in the followig will be also called *Zero to Forward* measure.
  The device is illuminated and is applied a varying potential, which sweeps from -0.5 V to 1.4 V, in the meantime the generated photocurrent is detected.

Scanning	Starting Bias (V)	Final Bias (V)	N°sweep points	Dwell time (ms)
$Z \rightarrow F$	-0.500	1.200	100	10

Table 4.5: Parameters for *Normal setting*

- *Reverse setting*, that in the followig will be also called *Forward to Zero* measure.
  It is the same of normal setting, but with the applied bias starting from maxima value to zero. In order to not stress the device, so to not acquire altered data before that the scanning starts, is applied the maxima bias for several seconds. This condition is obtained to set a variable delay in measure's configuration.

Scanning	Starting Bias (V)	Final Bias (V)	N°sweep points	Dwell time (ms)
$F \rightarrow Z$	1.200	-0.500	100	10

Table 4.6: Parameters for *Reverse setting*

∗ As will be presented in 5th chapter, for investigation of devices's performance, have been effectuate sequential J-V measurements. About this, it is important to note that after the first measure the following measure started as soon as velocity of operator, because the measuring system is not set for this kind of measure. For this reasons the time between one measure and the other, must be considered variable about several seconds.

4.2.2 Transient Photocurrent Measurement

As touched on in previous section and better explained in the following, during J-V measurement is emerged a hysterical behaviour of the tested devices. In order to try to clarify the nature and entity of the phenomena, is performed transient photocurrent measurement on the best devices. In particular has been studied the evolution in time of the photocurrent without any polarization applied to device(short circuit regime) on several dark-to-light cycles of one minute each. The measure starts with the device in dark. After the device is illuminated with one sun for one minute and simultaneously the photocurrent is recorded. At the end of minute the shutter is again closed for one minute before that another cycle starts. This sequence dark-to-light has been repeated for six times.

4.2.3 Scanning Electron Microscopy(SEM) Measurement

Principle of SEM

Scanning Electron Microscopy as all scanning technique is used in order to describe certain physical quantity as a function of position on the sample's surface. In particular, the probe in the SEM measurement is a focussed electron beam, having tuneable energy between 2-10 KeV and spot size until $1\mu m$ in the

top instrumentations. Due to dissimilar scattering events, the effect of incident beam, is the production of different kinds of reflected electrons, with which is possible investigate the simple surface topography or local surface analysis in terms of chemical composition. The intensity of emitted signals in different angles coming to the probed zone, determines the brightness of the spot on a video. The formation of a topographical image is due to local variations of electron emissivity of the surface.

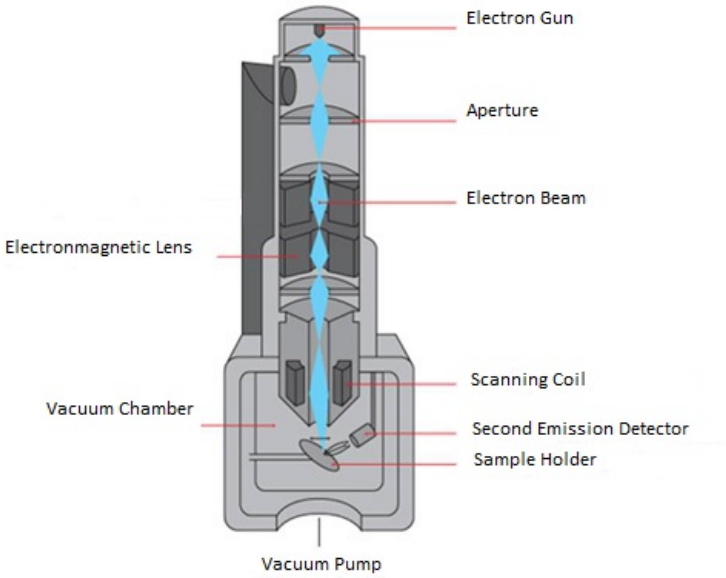

Figure 4.3: Schematic diagram of a scanning electron microscope (SEM)

4.2.4 Profilometer

The profilometer is used to obtain information about sample's surface, which are contained in *surface parameters*:

- *Roughness*: Closely spaced irregularities
- *Waviness*: More widely spaced irregularities
- *Error of Form*: Long period and non cyclic deviation
- *Amplitude Parameters*: Show in Table4.7

The profilometer are classified in *Non-contact Profilometers* and *Contact Profilometers*. The first type irradiates the sample with a beams of light and records the time pass between emission and return of reflected ray. The second

TERM	DEFINITION	USE
Ra	The roughness average (mean height)	Gives roughness of the machine surface the machine surface
Rq	RMS roughness	Describe the finish of optical surface
Rp and Rv	Max profile peak and max profile valley depth	Ra-info of friction and wear Rv- retaining of lubricant
Rt	Max height of surface	Gives overall roughness of the surface
Rz	Average max height of the profile	Evaluating surface texture on limited acces surfaces
Rsk	Skewness- measure of asymmetry of the profile about the mean line	Gives load carrying capacity, porosity characteristic of non-conventional machining process

Table 4.7: Amplitude parameters used in measurements by profilometer

type uses a sharp stylus which scans the surface maintaining a constant downward force. In order to maintain the constant force during the scan, the machine moves the stylus up an down producing height data. These profilometer no require measuring model and are easier to use than Non-contac profilometers. In the other hand Contact type show worse performances about resolution and speed of measurement.

4.2.5 UV-VIS Spectroscopy

The spectroscopic technics are based on exchange of energy which occurs between radiation and material. In particular the UV-VIS spectrophotometry regards absorbing phenomenon about lighting radiations belongs to *visible*(350-700nm) and *near ultraviolet* (200-350nm) ranges. Although is also possible to probe in *far ultraviolet*, when is available measurements in vacuum conditions. The measurement is realized to irradiate the sample with a monochromatic beam having known intensity and measuring the intensity of transmitted ray. The different absorption depending to every wavelength defines the peculiar absorption spectra of the probed material. In general the spectrophotometer UV-VIS can be adopted to extract qualitative information as pureness or presence of materials, otherwise more quantitative information as their concentration.

The quantitative determinations are based *Lambert-Beer law*, which asserts that the *absorbance* is equal to:

$$A = \xi cd$$

Where ξ is *molar extinction coefficient*, c is the concentration and d is thick

of the illuminated material. In particular, referring to intensity of incident intensity (I_0) and transmitted intensity (I) the *absorbance* is given to:

$$A = \log\left(\frac{I_0}{I}\right)$$

Therefore measuring the ratio ($\frac{I_0}{I}$), knowing thick and ξ, is possible to extract the concentration of a particular material.

Set up Measurement

In this work the UV-VIS spectrometry is been used in order to define the making process which produces the polymeric matrix containing the greatest amount of MoS_2. In particular are been tested samples made up PVP matrix containing flakesMoS_2 on glass substrate.
Between the different samples obtained by spin coating, is been changed concentration of polymer, speed and acceleration of rotation in deposition phases. In addition to samples of interest, has been necessary to execute absorption spectrums also of MoS_2 solution and its solvent, in order to identify the characteristic peaks ofMoS_2.
According to preliminary results about correlation between, PVP concentration and thick of matrix, obtained by profilometer, the UV-VIS absorption studies have been concentrated on samples make up by spin-coating on flight and having PVP concentration grater than $50\frac{mg}{ml}$.
The measurements are been performed using *UV/VIS/NIR Spectrophotometer Lambda 1050* with scan of wavelengths from $800nm$ to $400nm$ with a resolution of $2nm$.

PVP Concentration($\frac{mg}{ml}$)	Speed(rpm)
20	2000
60	2000 3500
100	2000 3500 6000
100 $*$	2000

Table 4.8: Samples tested in UV-VIS spectroscopy. All samples have been obtained by spin coating on flight, changing PVP concentration and speed of deposition.
The sample labeled as 100 $*$ identifies PVP without MoS_2, necessary to discriminate MoS_2's contributions

Chapter 5

Results and Analysis

The presentation of results will follows the order with which has been developed the thesis's activity, which can been separated in three sections.
In the first phase, the work was focused on fabrication of high performing classical MSSC based on Pervskite. In order to reach this target have been realized many devices, attempting at every turn to improve the "know how", so to improve their efficiency.
Subsequently, being the final aim that to replace the classical HTL (Spiro-OMeTAD) with MoS_2, the attention was transferred on research of best process to obtain the new structure. With this purpose were carried out several studies on physics characteristics, first just on flakes deposition and then on flakes contained in insulating matrix.
In the third phase, using the information extracted through preliminary studies, we tried to fabricate operating MSSC using flakes of MoS_2 as hole transport material. Every production run was tested by J-V measurement, in order to understand the problem, so to try to solve them through optimization of the processes.
Out of the primary targets of the thesis's work, has been also investigated through transient photocurrent measures, the strange behaviour of the photocurrent was appearing during the tests.

5.1 Classical MSSC Based On Perovskite

The *Classical J-V measurements* effectuated on the first production run did not show important performance, with efficiency which never exceed 1% and FF lower than 50, due to light S-shape of J-V curve. This behaviour indicates consistent leakage of photon generated carriers, that in this case can been imputable to poor quality of compact layer of TiO_2. Since to second run, the general per-

formance of the cells enhanced, showing FF exceeding 70 and reached efficiency grater than 2%. Below in Figure5.1 is showed the J-V curve of the best device, whose parameteres are reported in Table5.1

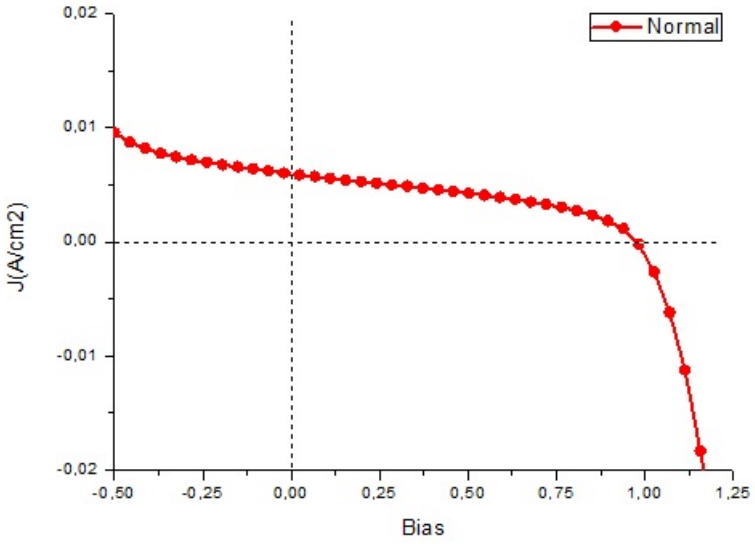

Figure 5.1: J-V curve of the best device tested with Normal setting

V_{oc} (V)	$J_{sc}(\frac{mA}{cm^2})$	FF	Efficiency
0.975	5.8058	40.8	2.3570

Table 5.1: Parameters of the best device tested with *Classical J-V measurements*

However, during our tests we causally noticed that if the pixel was tested more than once, its efficiency progressive improved until a "saturation" value reached after many measure cycles. In order to investigate this phenomena we tried to test many times the devices. In Figure5.2 are reported the J-V curves of the same pixel testes in *Normal Measure* setting, with respective parameters in Table5.2.

Measure	V_{oc} (V)	$J_{sc}(\frac{mA}{cm^2})$	FF	Efficiency
1	0.972	4.0388	67.0	4.0388
2	1.000	7.082	68.3	4.9406
3	1.030	8.208	66.5	5.6178
4	1.007	8.436	67.7	5.8670
5	1.008	8.555	68.1	5.9945
6	1.008	8.620	68.6	6.0818
7	1.008	8.916	60.0	6.3325

Table 5.2: Parameters for same pixel sequentially tested

As it is lighted by values in Table5.2, these sequential measurements induce

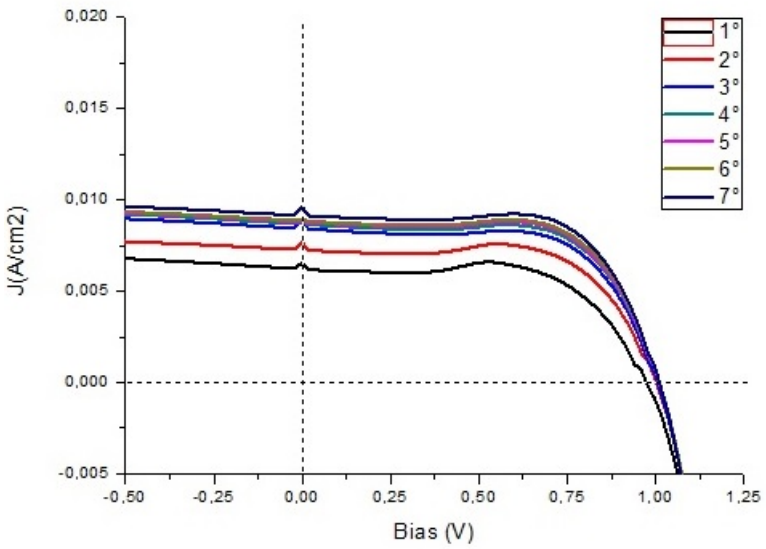

Figure 5.2: Sequential J-V curves of same pixel

an enhancement of efficiency mainly due to increment of photocurrent, since that the V_{oc} has little variations. At the beginning these observations have been driven us to think that the boost in photocurrent was due to a larger exposition time at light, resulting by consecutively measurements. Indeed, exist other kinds of devices, as dey-sentitized and organic solar cell,which show an enhance of their performance when a preexposure to light (so called *light soaking*) is effectuated before the measurements.
This behaviour is attributed to photoinduced doping or alterations of the electronic states on the surfaces of metal oxide layers employed [4]. In addition to this, a stronger phenomena with the same trend, has been observed effectuating measurements having different durations. In particular starting with classical measure, having 100 sweep points, then decreasing them up to 15.
Below Figure5.3 are reported other four measures having different durations, effectuated on the same device tested in the sequential measures showed before. The different curves are obtained decreasing the number of sweep points, so reducing the total measure's time.

N° sweep points	V_{oc} (V)	$J_{sc}(\frac{mA}{cm^2})$	FF	Efficiency
100	1.008	8.916	60.0	6.3325
50	1.037	11.339	71.52	8.5807
25	1.054	14.8417	61.4	9.8006

Table 5.3: Parameters for same pixel tested with different sweep points

As in sequential measures, it is evident an increase of photocurrent which

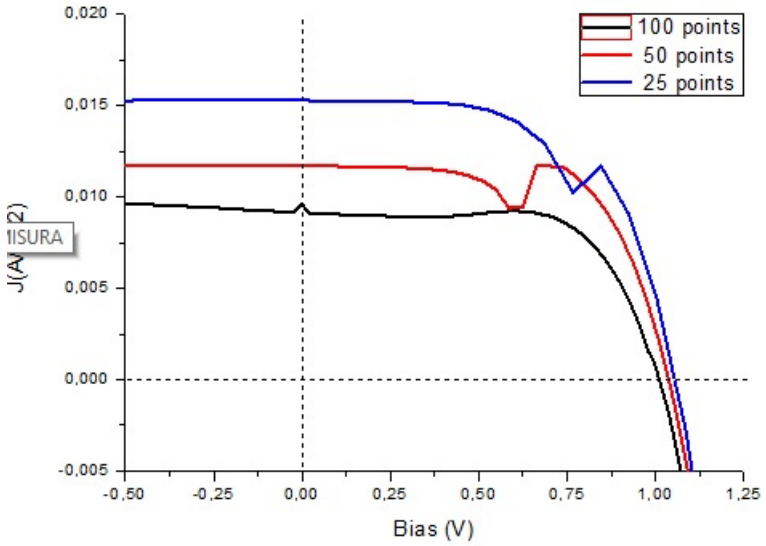

Figure 5.3: J-V curves obtained with different measure's time

corresponds to enhance of efficiency, that in this case reaches 9.8% although with imperfect J-V curves. This behaviour showed the existence of an unknown dependence of photocurrent to dynamics of potential applied. This dependence is well highlighted by an anomalous hysteresis, which manifests when two sequential J-V measurements are effectuated, before scanning from zero to forward bias and than viceversa. Indeed the best performance has been recorded with *Strained Measurement*, in which the same pixel of the same device showed an efficiency of 10.04%.
In figureFigure5.4 are plotted the J-V curves obtained with *Zero to Forward* scannig and with *Forward to Zero* scanning.

Kind of scanning	V_{oc} (V)	$J_{sc}(\frac{mA}{cm^2})$	FF	Efficiency
$Z \rightarrow F$	0.975	5.8058	40.8	2.3570
$F \rightarrow Z$	1.060	16.726	55.5	10.039

Table 5.4: Parameters for same pixel tested before with *Zero to Forward* ($Z \rightarrow F$) scannig and with *Forward to Zero* ($F \rightarrow Z$) scanning.Note that the maxima bias was applied for 30sec before that the reverse measure started

The hysteric behaviours, due to differences in the shape of the J-V curves derived by forward and reverse scanning, typically is attributed to the capacitance of the solar cell. Indeed if the scanning is done too fast, the charges stored in device, will be release as an extra current during reverse scanning. Although in very recent work, has been highlighted that in several technologies, using Perovskite as absorber, show stronger hysteresis also at very slow scanning [4].

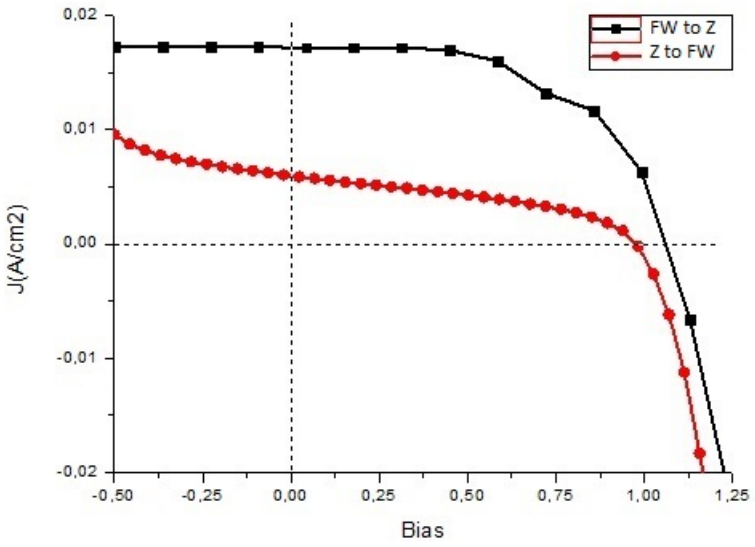

Figure 5.4: Different J-V curves for same pixel tested with *Zero to Forward* scannig (red) and then with *Forward to Zero* scanning (black)

The study have yet to examine in depth, but to this day, is thought that the phenomena is strongly correlated to architecture of device and its respective Perovskite p- and n- interfaces, which can create more or less surface states. In particular have been suggested three different possible origins, which may be uniquely responsible or all contributing to the effect:

- The Perovskite should presented very large defect density at surface of the material, generating interface states. These states traps the carriers during the forward scanning and then slowly release them during reverse scanning.
- The organometal trihalide perovskites posses ferroelectric properties, so a slow polarization of the material may occour. This polarization could have several influences, including making charge collection more or less favourable at the contacts.
- Due to process to obtain the Pervskite itself, may be present excess ions, as interstitial defects (iodide or methylammonium). During operation the interstitial ions could be able to migrate to either side of the film, screening space charge accumulations and incentivizing charge collection during operation.

5.2 Studies of MoS_2 Layer

The preliminary studies on MoS_2 deposition have been made on glass substrate, in order to verify the real possibility to create a film constituted by MoS_2 flakes. The deposition tested was *drop casting* and *spin coating*.
From investigations with optical microscope is clear the impossibility to obtain an uniform film of MoS_2 flakes. Indeed in the case of spin coating, there are conglomerates of MoS_2 in peripheral zones with wide central zone lacking of material(Figure5.5(a)). While for drop casting there are only small crystallization zone (Figure5.5(b)).

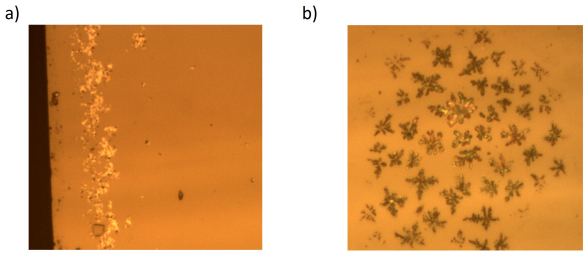

Figure 5.5: Investigation with optical microscope on deposition of MoS_2 flakes on glass substrate:(a)by spin coating and (b)by drop casting

Furthermore are given SEM images of MoS_2 flakes on Perovskite substrate, even with spin coating and drop casting deposition.
In Figure5.6 are reported the SEM image in which are observable the scarce presence of flakes on Pervskite islands.

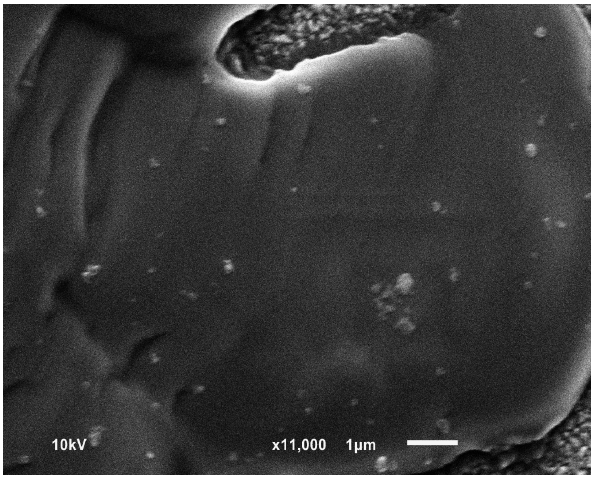

Figure 5.6: SEM image in which are distinguble the Perovskite islands on which are deposited very low amount of MoS_2 flakes

This both investigations prove the impossibility to create an uniform film

just with deposition of MoS_2 solution having this concentrations ($18\frac{mg}{l}$).
After these results our efforts are focused on realization of different architecture for use of MoS_2 as hole transport material.

5.3 Studies of MoS_2 in PVP Matrix

In this section will be showed the result obtained about the studies carry out in order to find the best process for realizations of PVP matrix containing the flakes of MoS_2. At the beginning the attention was focused on physics characteristics just of PVP film and at later stage of PVP/MoS_2 compound.

5.3.1 PVP film

The studies on physics characteristics of PVP are focused on thickness and homogenety, respectively using profilometer and optical microscope.

Homogeneity of PVP Film

From images given by optical microscope, emerge the strong dependence between concentration of polymer in solution, speed of deposition and uniformity of the resulting film. Indeed the presence of two solvents(water and ethanol) having strong difference in volatility, cause the creation of thin multilayer resulting in not uniform thickness of overall film, which shows accumulation zones of material. Typically, the film was thicker in the centre than the outlying zones. Effectuating many trials with different speed of deposition and different acceleration in spin coating process, emerged that the better uniformity in thickness of the sample is obtained with high speed and effectuating the spin coating on flight.

Thickness of PVP Film

After we obtained some information about method to make homogeneous film of PVP, the successive work was to obtain information on control of its thick. With this purpose have been tested with the profilometer the thickness of several samples made with different concentration of PVP and different speed of deposition. Below are reported the sample tested and the results of thickness depending on concentration of PVP (Table5.5) and depending on speed of rotation (Table5.6)
.

As consequence of the obtained results the conclusions, regarding just the physic characteristic of insulating matrix, is presumed that the optimal conditions of deposition are with relative high concentration (80-100($\frac{mg}{ml}$)) and speed

PVP Concentration($\frac{mg}{ml}$)	Thickness of Film (nm)
35	110
80	200
100	325

Table 5.5: Thickness measured of PVP film starting to a solution having different concentration. Every value of thickness is the averege on three measurements having an error of ±100nm.The speed of deposition is 3500rpm for every sample.

Speed (rpm)	Thickness of Film (nm)
1000	more than 1000
2000	750
3500	320
6000	160

Table 5.6: Thickness measured of PVP film changing speed of deposition. Every value of thickness is an avarege on three measurements having an error of ±100nm. The concentration of PVP is 100($\frac{mg}{ml}$) for every sample.

sufficient high to ensure good homogeneity and not too high thickness (3000-4000rpm).

5.3.2 UV-VIS Spectroscopy of PVP/MoS_2 Compound

In order to confirm the presence of the flakes within the matrix and to estimate their amount, are been conducted approximate spectroscopic studies. This has been useful to choose the more suitable process in fabrication of the devices. Preliminary tests have been conducted to extract the absorption spectra of MoS_2 flakes dispersed in solution and just film of PVP film on glass substrate. In the Figure5.7 are reported the spectra for MoS_2, which shows strong absorption for wavelength smaller than 500nm but however presents weaker absorption in range from 500nm to 700nm.

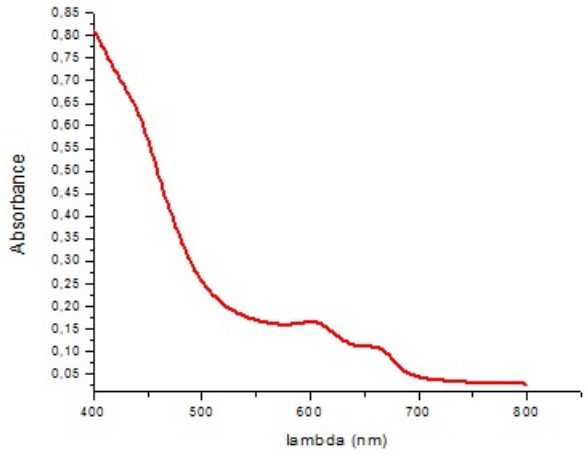

Figure 5.7: Absorption spectra of MoS_2 flakes dispesed in solution, having concentration 18mg/l

As showed in Figure5.8 the absorption spectra of PVP film is much weak due to its small thick (about1μm in the tested sample) and low absorption, giving a signal near to resolution limit.

Considering also the reduction of absorption of MoS_2 flakes within the PVP, due to small probed thick and lower concentration than MoS_2 in solution, can be made a comparison between spectra of PVP and PVP+ MoS_2 to obtain qualitative information.
Below are reported the spectra of MoS_2 within PVP obtained through different concentration of polymer (Figure5.9)and different speed of deposition(Figure5.10).

Due to uncertainity on many parameters, as thickness of PVP film depending both concentration and speed of deposition, homogeneity of probed point, very low concentration of MoS_2 flakes and working near to resolution limit, the extracted information from these measures must been considered extremely approximate.

In this viewpoint, from Figure5.9 it seems that for low concentration of polymer ($20(\frac{mg}{ml})$) the MoS_2 does not present, because it is preserved the characteristic minima of PVP's spectra. Increasing the concentration of PVP, so enhancing the viscosity of solution arise low pick of absorption about 550nm probably due to presence of MoS_2 flakes, although exist the possibility the it is due to an interference phenomena given by thick of film .
In Figure5.10 is presumed that the possible component of MoS_2 is present in 450-550 range. From these results, regarding the fabrication of the devices, we decided to mainly use concentration of PVP included between 30 and $110(\frac{mg}{ml})$ and deposition with speed between 3000 and 4000 rpm.

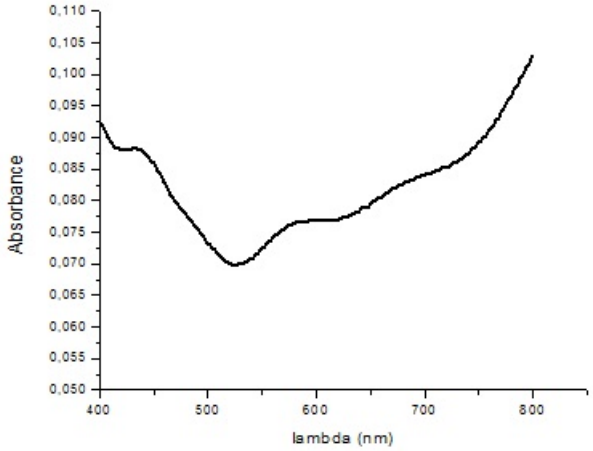

Figure 5.8: Absorption spectra of PVP film having a thickness about1μm, obtained by solution containing 100($\frac{mg}{ml}$) of polymer and spinned at 2000rpm

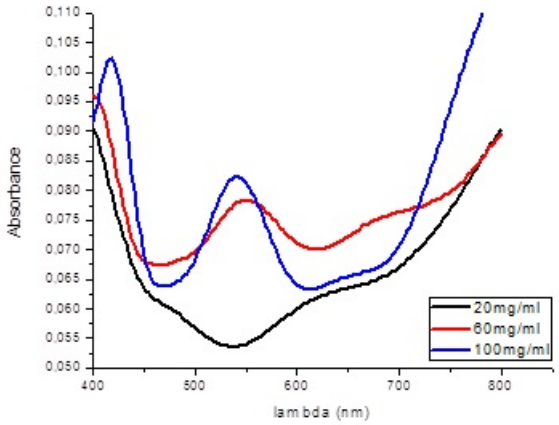

Figure 5.9: Absorption spectra of PVP+MoS_2 spinned at 2000rpm with different concentrations of polymer

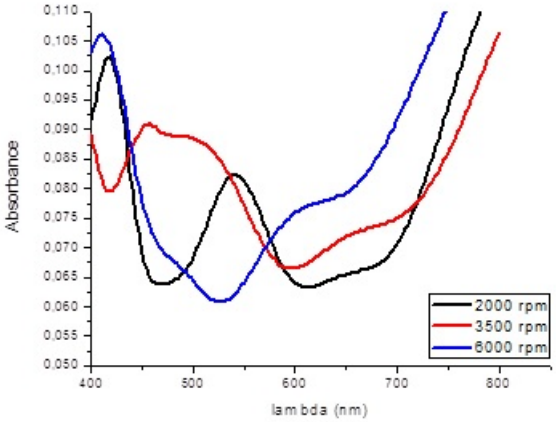

Figure 5.10: Absorption spectra of PVP+MoS_2 having 100($\frac{mg}{ml}$) of polymer and spinned at different speed

5.4 MSSC Based Pervskite Using MoS_2 as HTL

As say are been made many devices through different fabrication process, but in no case showing performance comparable to classical MSSC.
The devices were realized with relative high PVP concentration (80-110($\frac{mg}{ml}$)) and with different speed of deposition between 3000 and 4000rpm. The performance of all devices are very low, with efficiency that not exceed the two tenth. The performance of the best device are reported in Figure5.11 and Table5.7.

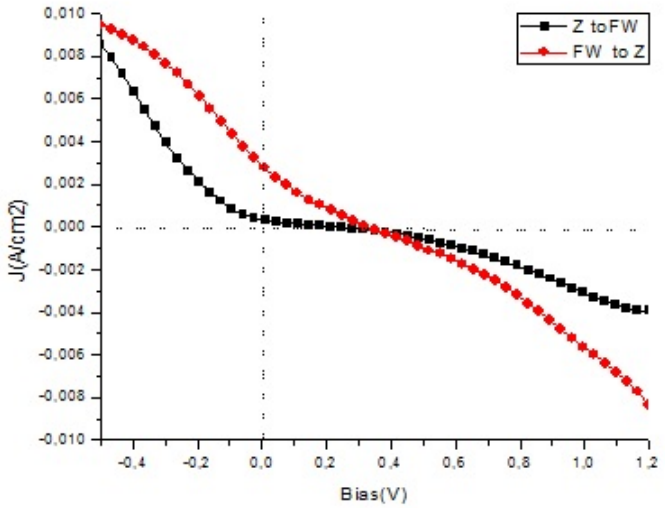

Figure 5.11: Different J-V curves for same pixel tested with *Zero to Forward* scannig (black) and with *Forward to Zero* scanning (red). The device has been obtained with 100($\frac{mg}{ml}$) spinned at 3500rpm.

Kind of scanning	V_{oc} (V)	$J_{sc}(\frac{mA}{cm^2})$	FF	Efficiency
$Z \rightarrow F$	0.228	0.343	19.1	0.0149
$F \rightarrow Z$	0.324	2.916	19.7	0.1848

Table 5.7: Parameters for same pixel tested before with *Zero to Forward* ($Z \rightarrow F$) scannig and then with *Forward to Zero* ($F \rightarrow Z$) scanning. Note that the maxima bias was applied for 60sec before that the reverse measure started

As in this case of the classical MSSC, also these devices presented a hysteresis in case of sequential measures (Zero-Forward then Forward-Zero), in which the better performance are showed by the latter measure.
All devices presented very low FF due to their strong S-shape, which testify the presence of not good realization of contact between Perovskite and back contact. This condition induce large leakage of photocurrent, because the photogenerated holes can not be collected, so they recombine with electron, reducing the overall

extracted current.

5.5 Transient Photocurrent Measure

As say in previous section, due to strong differences in the showed photocurrent, depending to methods of measure during test phases, suggested us to carry out to investigate on temporal dynamic of photocurrent.
This have been effectuated through *transient photocurrent measure* on operating Classical MSSC based on Perovskite at short circuit condition.
Below in Figure5.12 are reported the evolution of photocurrent during six cycles dark-light of the same tested pixel.

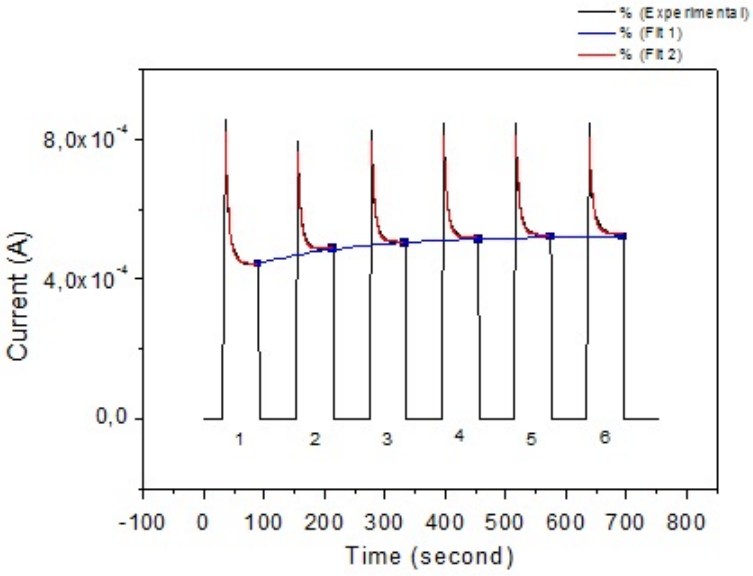

Figure 5.12: Dark/light cycle of one minute each(Black line: experimental data. Blue square: shutting-off point. Red line: decay exponential fit. Blue line: first order exponential growth.)

In the signal are clear two temporal evolutions, having both different trends and different characteristic length of time.
The faster, highlighted to red fit shows the impressive exponential decrease of the photocurrent just in few seconds. Although the nature of this phenomena is yet unknown, it seems to be the cause, for which the performance recorded with fast scanning in J-V measurements are better than those having slow scanning. Indeed with smaller measure time the photocurrent does not end its transient state, remaining at higher values.
The second evolution, much slower than the previous, identified by blue fit, shows a slightly enhance proceeding with the measures. This second trend,

can be related to thermal effect induced by prolonged time of exposition at light. This effect can be better observed in Figure5.13, in which are reported the evolution of photocurrent at a single exposition of duration equal to 1000 seconds.

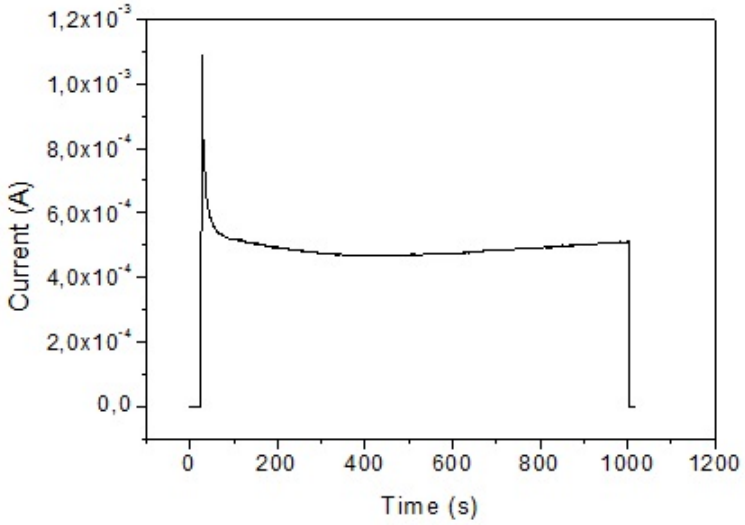

Figure 5.13: Transient photocurrent under one sun illumination over a 1000 second time scale

Chapter 6

Conclusion

Thanks to its excellent optoelectronic properties and its brilliant first application, the Metal-Halide Perovskite continue to been seen, as a great opportunity for the realization of solar cell at high performance and low cost, which be able to competitive with silicon technology.
To this day, many studies are carrying out, with the aim to find new material in order to improve the performance of actual architecture. In this sense, the attempt to substitute the Spiro with other material, as MoS_2 it is one of many pursuable directions.
Other studies are focusing on dynamic of photophysic in solar cell based on Perovskite, among which also the hysteresis observed in this work. As say in the previous chapter, the inducing causes of the hysteresis, have been related to conditions arising to interfaces between Perovskite and other material in the cell, as HTL and ETL. For this reasons several groups are working on possibility to reduce this effects creating solar cells based on Pervoskite without HTL, so totally committing the transport of the holes just to Perovskite, thanks to its good properties as p conductor.

Bibliography

[1] E. . E. P. I. Association, editor. *Global market outlook for photovoltaic until 2016.*

[2] C. D. D. C. R. Kagan, D. B. Mitzi. Organic-inorganic hybrid materials as semiconducting channels in thin-film field-effect transistors.

[3] Z. Cheng and J. Lin. Layered organic–inorganic hybrid perovskites: structure, optical properties, film preparation, patterning and templating engineering.

[4] J. M. B. G. E. E. T. L. N. K. N. S. D. S. J. T.-W. W. K. W. Henry J. Snaith, Antonio Abate and W. Zhang. Anomalous hysteresis in perovskite solar cells.

[5] J.-H. I. K.-B. L. T. M. A. M. S.-J. M. R. H.-B. J.-H. Y. J. E. M. M. G. . N.-G. P. Hui-Seon Kim, Chang-Ryul Lee. Lead iodide perovskite sensitized all-solid-state submicron thin film mesoscopic solar cell with efficiency exceeding 9%.

[6] J. H.-J. S. Kin Fai Mak, Changgu Lee and T. F. Heinz. Atomically thin mos2: A new direct-gap semiconductor.

[7] T. M.-T. N. M.-H. J. S. Michael M. Lee, Joël Teuscher. Efficient hybrid solar cells based on meso-superstructured organometal halide perovskites.

[8] D. M. K. Nadia Ameli. Energy for sustainable development.

[9] Y. H. L.-G. M. E.-M. G. M. K. N. Olga Malinkiewicz1, Aswani Yella and H. J. Bolink. Perovskite solar cells employing organic charge-transport layers.

[10] M. D.-G. E. E. . H. J. S. Pablo Docampo, James M. Ball. Efficient organometal trihalide perovskite planar-heterojunction solar cells on flexible polymer substrates.

[11] S. G. R. G. U. S. a. J. S. Pablo Docampo, Andrew Hey. Pore filling of spiro-ometad in solid-state dye-sensitized solar cells determined via optical reflectometry.

[12] F. F.-S. S. H. I. I. M.-S. J. B. Pablo P. Boix, Yong Hui Lee and S. I. Seok. From flat to nanostructured photovoltaics: Balance between thickness of the absorber and charge screening in sensitized solar cells.

[13] A. K. J. N. C. Qing Hua Wang, Kourosh Kalantar-Zadeh and M. S. Strano. Electronics and optoelectronics of two-dimensional transition metal dichalcogenides.

[14] G. G. C. M. M. J. P. A.-T. L. L. M. H. A. P.-H. J. S. Samuel D. Stranks, Giles E. Eperon. Electron-hole diffusion lengths exceeding 1 micrometer in an organometal trihalide perovskite absorber.

[15] J.-S. L. E. D. P. A. L. G. Sanjun Zhanga, Gaëtan Lantya. Synthesis and optical properties of novel organic–inorganic hybrid nanolayer structure semiconductors.

[16] T. C. Sum1 and N. Mathews. Advancements in perovskite solar cells: Photophysics behind the photovoltaics.